

## Solution NMR Studies of the $A\beta(1-40)$ and $A\beta(1-42)$ Peptides Establish that the Met35 Oxidation State Affects the Mechanism of Amyloid Formation

Liming Hou,<sup>†</sup> Haiyan Shao,<sup>†</sup> Yongbo Zhang,<sup>†</sup> Hua Li,<sup>†</sup> Nanda K. Menon,<sup>‡</sup> Elizabeth B. Neuhaus,<sup>‡</sup> John M. Brewer,<sup>‡</sup> In-Ja L. Byeon,<sup>§</sup> Dale G. Ray,<sup>†</sup> Michael P. Vitek,<sup>||</sup> Takashi Iwashita,<sup>⊥</sup> Ronald A. Makula,<sup>‡</sup> Alan B. Przybyla,<sup>‡</sup> and Michael G. Zagorski<sup>\*†</sup>

Contribution from the Department of Chemistry, Case Western Reserve University, Cleveland, Ohio 44106-7078, Department of Biochemistry, University of Georgia, Athens, Georgia 30602, Department of Chemistry, Chemical Instrumentation Center, The Ohio State University, Columbus, Ohio 43210, Department of Neurology, Duke University Medical Center, Durham, North Carolina 27710, and Suntory Institute of Bioorganic Research, Wakayamadai, Shimamoto-cho, Mishima-gun, Osaka 618, Japan

Received June 21, 2003; E-mail: mxz12@po.cwru.edu

**Abstract:** The pathogenesis of Alzheimer's disease is characterized by the aggregation and fibrillation of the 40-residue  $A\beta(1-40)$  and 42-residue  $A\beta(1-42)$  peptides into amyloid plaques. The structural changes associated with the conversion of monomeric  $A\beta$  peptide building blocks into multimeric fibrillar  $\beta$ -strand aggregates remain unknown. Recently, we established that oxidation of the methionine-35 side chain to the sulfoxide ( $\text{Met35}^{\text{red}} \rightarrow \text{Met35}^{\text{ox}}$ ) significantly impedes the rate of aggregation and fibrillation of the  $A\beta$  peptide. To explore this effect at greater resolution, we carefully compared the  $^1\text{H}$ ,  $^{15}\text{N}$ , and  $^{13}\text{C}$  NMR chemical shifts of four  $A\beta$  peptides that had the Met35 reduced or oxidized ( $A\beta(1-40)\text{Met35}^{\text{red}}$ ,  $A\beta(1-40)\text{Met35}^{\text{ox}}$ ,  $A\beta(1-42)\text{Met35}^{\text{red}}$ , and  $A\beta(1-42)\text{Met35}^{\text{ox}}$ ). With the use of a special disaggregation protocol, the highly aggregation prone  $A\beta$  peptides could be studied at higher, millimolar concentrations (as required by NMR) in aqueous solution at neutral pH, remaining largely monomeric at 5 °C as determined by sedimentation equilibrium studies. The NOE, amide-NH temperature coefficients, and chemical shift indices of the  $^1\text{H}\alpha$ ,  $^{13}\text{C}\alpha$ , and  $^{13}\text{C}\beta$  established that the four peptides are largely random, extended chain structures, with the  $\text{Met35}^{\text{ox}}$  reducing the propensity for  $\beta$ -strand structure at two hydrophobic regions (Leu17–Ala21 and Ile31–Val36), and turn- or bendlike structures at Asp7–Glu11 and Phe20–Ser26. Additional NMR studies monitoring changes that occur during aging at 37 °C established that, along with a gradual loss of signal/noise, the  $\text{Met35}^{\text{ox}}$  significantly hindered upfield chemical shift movements of the 2H NMR signals for the His6, His13, and His14 side chains. Taken together, the present NMR studies demonstrate that the  $\text{Met35}^{\text{red}} \rightarrow \text{Met35}^{\text{ox}}$  conversion prevents aggregation by reducing both hydrophobic and electrostatic association and that the  $A\beta(1-40)\text{Met35}^{\text{red}}$ ,  $A\beta(1-40)\text{Met35}^{\text{ox}}$ ,  $A\beta(1-42)\text{Met35}^{\text{red}}$ , and  $A\beta(1-42)\text{Met35}^{\text{ox}}$  peptides may associate differently, through specific, sharp changes in structure during the initial stages of aggregation.

### Introduction

Alzheimer's disease (AD) is the most common cause of adult-onset dementia and in the United States affects approximately 10–15% of individuals over age 65 and up to 48% over the age 80.<sup>1</sup> The neuropathological features of AD are the extracellular deposition of the  $A\beta$  peptide as amyloid plaques (amyloidosis) and the presence of intraneuronal neurofibrillary tangles.<sup>2</sup> The amyloid plaques are characterized by distinct

tinctorial properties and fibrils of 7–10 nm in diameter, with the aggregated  $A\beta$  peptide adopting a cross- $\beta$ -pleated sheet structure.<sup>3</sup> Recent solid-state NMR data demonstrated that the  $A\beta$  peptide adopts the less common parallel  $\beta$ -strand orientation in the amyloid fibrils.<sup>4,5</sup>

The association or  $\beta$ -aggregation of proteins to produce amyloid is a subject of intense research interest, due to the role of protein self-assembly in normal function, and because of the possible involvement of protein misassembly in the pathology

<sup>†</sup> Case Western Reserve University.

<sup>‡</sup> University of Georgia.

<sup>§</sup> The Ohio State University.

<sup>||</sup> Duke University Medical Center.

<sup>⊥</sup> Suntory Institute of Bioorganic Research.

(1) Conway, K. A.; Baxter, E. W.; Felsenstein, K. M.; Reitz, A. B. *Curr. Pharm. Des.* **2003**, *9*, 427–447.

(2) Trojanowski, J. Q.; Lee, V. M. *Ann. N.Y. Acad. Sci.* **2000**, *924*, 62–67.

(3) Kirschner, D. A.; Abraham, C.; Selkoe, D. J. *Proc. Natl. Acad. Sci. U.S.A.* **1986**, *83*, 503–507.

(4) Benzinger, T. L.; Gregory, D. M.; Burkoth, T. S.; Miller-Auer, H.; Lynn, D. G.; Botto, R. E.; Meredith, S. C. *Biochemistry* **2000**, *39*, 3491–3499.

(5) Petkova, A. T.; Ishii, Y.; Balbach, J. J.; Antzutkin, O. N.; Leapman, R. D.; Delaglio, F.; Tycko, R. *Proc. Natl. Acad. Sci. U.S.A.* **2002**, *99*, 16742–16747.

of certain diseases such as AD and scrapie.<sup>6–8</sup> In addition, de novo designed peptides and other naturally occurring proteins, not associated with human disease, can be induced to form amyloid fibrils, indicating that amyloidosis may be a generic property of all peptides and proteins.<sup>9</sup> Despite over a decade of research efforts, the molecular mechanisms of amyloidosis remain largely unknown, which is partly due to the lack of high-resolution structural data.

The amyloid  $A\beta$  is a normally secreted, small peptide (~4 kDa) that results from processing of a larger amyloid precursor protein (APP). Extensive genetic and cell viability studies support a key role for the  $A\beta$  peptide in AD neurodegeneration and oxidative stress. The  $A\beta$  peptide becomes neurotoxic to cortical cell cultures when aggregated as amyloid-like  $\beta$ -strand structures,<sup>10,11</sup>  $A\beta$  protofibrils,<sup>12</sup> or other aggregates such as  $A\beta$  derived diffusible ligands that kill mature neurons at nanomolar concentrations and cause neurological dysfunction in the hippocampus.<sup>13</sup> The two major  $A\beta$  peptides are the 40-residue  $A\beta(1-40)$  and the 42-residue  $A\beta(1-42)$ , which differ in the absence or presence of two extra C-terminal residues (Ile41–Ala42). The N-terminal (residues 1–28) residues comprise a hydrophilic domain with a high proportion of charged residues (46%), whereas the C-terminal domain (residues 29–40 or 29–42) is completely hydrophobic and is presumably associated with the cell membrane of APP. Although the  $A\beta(1-40)$  and  $A\beta(1-42)$  peptides are ubiquitous in biological fluids of humans (at an approximate ratio of 9:1), it is thought that the longer  $A\beta(1-42)$  is more pathogenic, due to its higher quantities in the amyloid plaques of sporadic AD cases, its even higher quantities in patients afflicted with early-onset AD,<sup>14,15</sup> and because of the greater in vitro tendency of the  $A\beta(1-42)$  to aggregate and precipitate as amyloid.<sup>16,17</sup>

The single methionine located at position 35 (Met35) of the  $A\beta$  plays an important role in AD-associated oxidative stress and may act as an electron donor for the reduction of  $A\beta$ -bound  $Cu^{II}$  to  $Cu^I$ .<sup>18–20</sup> For many proteins, the methionine side chains are easily oxidized to the sulfoxide under physiological conditions ( $Met^{red} \rightarrow Met^{ox}$ ) and may function as endogenous antioxidants.<sup>20,21</sup> Oxidized Met35 ( $Met35^{ox}$ ) comprises 10–50% of total brain  $A\beta$  in post-mortem AD plaques<sup>22</sup> and thus may

be related to AD-related oxidative stress events. Recent Raman spectroscopic analysis of AD brain tissue confirmed that the Met35 is extensively oxidized and that Zn(II) and Cu(II) are coordinated to the histidine residues, thus providing a chemical basis for the extensive oxidative damage caused by the  $A\beta$  peptide in AD.<sup>23</sup>

In previous work, using circular dichroism (CD), thioflavin-T binding amyloid assay, atomic force microscopy (AFM), and mass spectrometry (MS), we and others demonstrated that the  $A\beta(1-40)Met35^{ox}$  and  $A\beta(1-42)Met35^{ox}$  peptides undergo  $\beta$ -aggregation at significantly reduced rates, as compared to the  $A\beta$  peptides containing  $Met35^{red}$ .<sup>24–26</sup> Most significantly, the  $Met35^{ox}$  prevented formation of the  $A\beta$  protofibril, which is believed to be a common, toxic intermediate in the amyloidosis of many proteins. Our working hypothesis is that this inhibition may be due to the increased polarity imparted by the  $Met35^{ox}$  side chain at the hydrophobic C-terminus.

To further investigate the relationship between the  $Met35$  oxidation state and  $A\beta$ -aggregation, here we utilized NMR spectroscopy to obtain site-specific structural information. Although several NMR reports have already been described for the  $A\beta$  peptide in solution, these studies were done under varied conditions (pH, temperature, buffer, ionic strength, aqueous solutions – with or without organic cosolvents and detergents), and with peptides of dissimilar lengths and  $Met35$  oxidation states.<sup>24,27–35</sup> Because of the extreme sensitivity of the  $A\beta$  peptide structure with the extrinsic solution conditions,<sup>36</sup> the NMR studies here utilized a single set of conditions (aqueous solution, pH 7.2, 5 °C) for analysis of four  $A\beta$  peptides with different  $Met35$  oxidation states ( $A\beta(1-40)Met35^{red}$ ,  $A\beta(1-40)Met35^{ox}$ ,  $A\beta(1-42)Met35^{red}$ , and  $A\beta(1-42)Met35^{ox}$ ). To overcome the intrinsic structure and aggregation variability among the different  $A\beta$  peptide lots,<sup>36,37</sup> all pre-aggregated seed material was carefully removed before sample preparation.<sup>38</sup> This procedure enabled detection of the monomeric state and

(6) Wetzel, R. *Adv. Protein Chem.* **1997**, *50*, 183–242.

(7) Fink, A. L. *Fold Des.* **1998**, *3*, R9–23.

(8) Thirumalai, D.; Klimov, D.; Dima, R. *Curr. Opin. Struct. Biol.* **2003**, *13*, 146–159.

(9) Chiti, F.; Webster, P.; Taddei, N.; Clark, A.; Stefani, M.; Ramponi, G.; Dobson, C. M. *Proc. Natl. Acad. Sci. U.S.A.* **1999**, *96*, 3590–3594.

(10) Simmons, L. K.; May, P. C.; Tomaselli, K. J.; Rydel, R. E.; Fuson, K. S.; Brigham, E. F.; Wright, S.; Lieberburg, I.; Becker, G. W.; Brems, D. N.; Li, W. *Mol. Pharmacol.* **1994**, *45*, 373–379.

(11) Walsh, D. M.; Klyubin, I.; Fadeeva, J. V.; Cullen, W. K.; Anwyl, R.; Wolfe, M. S.; Rowan, M. J.; Selkoe, D. J. *Nature* **2002**, *416*, 535–539.

(12) Hartley, D. M.; Walsh, D. M.; Ye, C. P.; Diehl, T.; Vasquez, S.; Vassilev, P. M.; Teplow, D. B.; Selkoe, D. J. *J. Neurosci.* **1999**, *19*, 8876–8884.

(13) Klein, W. L.; Krafft, G. A.; Finch, C. E. *Trends Neurosci.* **2001**, *24*, 219–224.

(14) Gravina, S. A.; Ho, L.; Eckman, C. B.; Long, K. E.; Otvos, L., Jr.; Younkin, L. H.; Suzuki, N.; Younkin, S. G. *J. Biol. Chem.* **1995**, *270*, 7013–7016.

(15) Hardy, J. *Trends Neurosci.* **1997**, *20*, 154–159.

(16) Barrow, C. J.; Zagorski, M. G. *Science* **1991**, *253*, 179–182.

(17) Harper, J. D.; Lansbury, P. T. *Annu. Rev. Biochem.* **1997**, *66*, 385–407.

(18) Huang, X.; Cuajungco, M. P.; Atwood, C. S.; Hartshorn, M. A.; Tyndall, J. D.; Hanson, G. R.; Stokes, K. C.; Leopold, M.; Multhaup, G.; Goldstein, L. E.; Scarpa, R. C.; Saunders, A. J.; Lim, J.; Moir, R. D.; Glabe, C.; Bowden, E. F.; Masters, C. L.; Fairlie, D. P.; Tanzi, R. E.; Bush, A. I. *J. Biol. Chem.* **1999**, *274*, 37111–37116.

(19) Varadarajan, S.; Kanski, J.; Aksenova, M.; Lauderback, C.; Butterfield, D. A. *J. Am. Chem. Soc.* **2001**, *123*, 5625–5631.

(20) Schoneich, C. *Arch. Biochem. Biophys.* **2002**, *397*, 370–376.

(21) Levine, R. L.; Mosoni, L.; Berlett, B. S.; Stadtman, E. R. *Proc. Natl. Acad. Sci. U.S.A.* **1996**, *93*, 15036–15040.

(22) Kuo, Y. M.; Kokjohn, T. A.; Beach, T. G.; Sue, L. I.; Brune, D.; Lopez, J. C.; Kalback, W. M.; Abramowski, D.; Sturchler-Pierrat, C.; Staufenbiel, M.; Roher, A. E. *J. Biol. Chem.* **2001**, *276*, 12991–12998.

(23) Dong, J.; Atwood, C. S.; Anderson, V. E.; Siedlak, S. L.; Smith, M. A.; Perry, G.; Carey, P. R. *Biochemistry* **2003**, *42*, 2768–2773.

(24) Watson, A. A.; Fairlie, D. P.; Craik, D. J. *Biochemistry* **1998**, *37*, 12700–12706.

(25) Palmblad, M.; Westlind-Danielsson, A.; Bergquist, J. *J. Biol. Chem.* **2002**, *277*, 19506–19510.

(26) Hou, L.; Kang, I.; Marchant, R. E.; Zagorski, M. G. *J. Biol. Chem.* **2002**, *277*, 40173–40176.

(27) Talafous, J.; Marcinowski, K. J.; Klopman, G.; Zagorski, M. G. *Biochemistry* **1994**, *33*, 7788–7796.

(28) Sticht, H.; Bayer, P.; Willbold, D.; Dames, S.; Hilbich, C.; Beyreuther, K.; Frank, R. W.; Röscher, P. *Eur. J. Biochem.* **1995**, *233*, 293–298.

(29) Kohno, T.; Kobayashi, K.; Maeda, T.; Sato, K.; Takashima, A. *Biochemistry* **1996**, *35*, 16094–16104.

(30) Coles, M.; Bicknell, W.; Watson, A. A.; Fairlie, D. P.; Craik, D. J. *Biochemistry* **1998**, *37*, 11064–11077.

(31) Shao, H.; Jao, S.-C.; Ma, K.; Zagorski, M. G. *J. Mol. Biol.* **1999**, *285*, 755–773.

(32) Zhang, S.; Iwata, K.; Lachenmann, M. J.; Peng, J. W.; Li, S.; Stimson, E. R.; Lu, Y.; Felix, A. M.; Maggio, J. E.; Lee, J. P. *J. Struct. Biol.* **2000**, *130*, 130–141.

(33) Jarvet, J.; Damberg, P.; Bodell, K.; Eriksson, L. E. G.; Gräslund, A. *J. Am. Chem. Soc.* **2000**, *122*, 4261–4268.

(34) Riek, R.; Guntert, P.; Dobeli, H.; Wipf, B.; Wuthrich, K. *Eur. J. Biochem.* **2001**, *268*, 5930–5936.

(35) Crescenzi, O.; Tomaselli, S.; Guerrini, R.; Salvadori, S.; D'Ursi, A. M.; Temussi, P. A.; Picone, D. *Eur. J. Biochem.* **2002**, *269*, 5642–5648.

(36) Zagorski, M. G.; Yang, J.; Shao, H.; Ma, K.; Zeng, H.; Hong, A. *Amyloid, Prions, and Other Protein Aggregates*; Academic Press: New York, 1999; Vol. 309, pp 189–204.

(37) Soto, C.; Castaño, E. M.; Kumar, R. A.; Beavis, R. C.; Frangione, B. *Neurosci. Lett.* **1995**, *200*, 105–108.

(38) Fezoui, Y.; Hartley, D.; Harper, J.; Khurana, R.; Walsh, D.; Condron, M.; Selkoe, D.; Lansbury, P.; Fink, A.; Teplow, D. *Amyloid: Int. J. Exp. Clin. Invest.* **2000**, *7*, 166–178.

enabled NMR analysis of the highly aggregation prone A $\beta$ (1–42)Met35<sup>red</sup>, as well as the <sup>1</sup>H, <sup>15</sup>N, <sup>13</sup>C $\alpha$ , and <sup>13</sup>C $\beta$  chemical shift assignments of all four peptides.

Overall, the NMR data support the absence of any well-defined secondary or tertiary structures, in that all four peptides are largely random, extended chains. However, on the basis of NOE and chemical shift data, the A $\beta$ (1–40)Met35<sup>red</sup> and A $\beta$ (1–42)Met35<sup>red</sup> peptides have residual  $\beta$ -strand structure at two hydrophobic regions (Leu17–Ala21 and Ile31–Val36) and turn- or bendlike structures at two largely hydrophilic regions (Asp7–Glu11 and Phe20–Ser26). Aging studies performed at 37°C demonstrate that the Met35<sup>ox</sup> reduces gradual upfield chemical shift movements of the 2H NMR signals for the His6, His13, and His14 side chains. On the basis of these data, we propose that the Met35<sup>red</sup>  $\rightarrow$  Met35<sup>ox</sup> conversion inhibits amyloid formation by preventing early, site-specific hydrophobic and electrostatic associations and that different association steps may be involved in amyloid formation for the A $\beta$ (1–40) and A $\beta$ (1–42) peptides, respectively. The implications of these results to unraveling a molecular mechanism of amyloidosis and the relationship between A $\beta$ -aggregation and oxidative stress are discussed.

## Experimental Procedures

**Sample Preparation.** Synthetic A $\beta$  peptides were prepared using standard Fmoc chemistry on an automated (Applied Biosystems 433A) synthesizer. The primary amino acid sequence for the amyloid A $\beta$ (1–42) peptide is the following: H<sub>3</sub>N<sup>+</sup>–D<sup>1</sup>–A–E–F–R<sup>5</sup>–H–D–S–G–Y<sup>10</sup>–E–V–H–H–Q<sup>15</sup>–K–L–V–F–F<sup>20</sup>–A–E–D–V–G<sup>25</sup>–S–N–K–G–A<sup>30</sup>–I–I–G–L–M<sup>35</sup>–V–G–G–V–V<sup>40</sup>–I–A<sup>42</sup>–COO<sup>–</sup>. The amyloid A $\beta$ (1–40) peptide has the identical sequence, except that the last two C-terminal residues (Ile41 and Ala42) are absent. Site-specific or uniformly (>95%) <sup>15</sup>N-labeled peptides were prepared by chemical synthesis using <sup>15</sup>N-labeled Fmoc protected amino acids (Cambridge Isotopes) or biosynthetically from *E. coli* as a recombinant fusion protein in minimal media containing <sup>15</sup>NH<sub>4</sub>Cl as the sole nitrogen source for singly, uniformly <sup>15</sup>N-labeled, and both <sup>15</sup>NH<sub>4</sub>Cl- and <sup>13</sup>C-labeled glucose (U-<sup>13</sup>C<sub>6</sub>) for uniformly doubly <sup>15</sup>N- and <sup>13</sup>C-labeled A $\beta$ (1–40)Met35<sup>red</sup> and A $\beta$ (1–42)Met35<sup>red</sup> (Recombinant Peptides). The A $\beta$ (1–40)Met35<sup>ox</sup> and A $\beta$ (1–42)Met35<sup>ox</sup> were prepared by H<sub>2</sub>O<sub>2</sub> oxidation of A $\beta$ (1–40)Met35<sup>red</sup> and A $\beta$ (1–42)Met35<sup>red</sup> peptides.<sup>26</sup> To avoid inadvertent Met35 oxidation, all solvents were carefully degassed, and the dry peptides were stored under an inert N<sub>2</sub> atmosphere (–70°C). The A $\beta$ (1–42)Met35<sup>red</sup> is particularly sensitive to oxidation,<sup>39</sup> which can occur during storage in solvents such as dimethyl sulfoxide where both oxidation<sup>40</sup> and fibrillation have been seen.<sup>41</sup> The peptides were purified by HPLC using the following columns: (1) Zorbax 300-SB-C8 semipreparative column (9.4 mm i.d. x 250 mm L) containing StableBond packing material of octyl stationary phase (Rockland Technologies), or (2) Vydac 259-VHP822 preparative column (22 mm i.d. x 250 mm L) containing highly cross-linked polystyrene–divinylbenzene copolymer beads with 300 Å pores (Separation Group). The solvent system consisted of a linear gradient of 20–80% acetonitrile in water, that contained either 0.1–0.08% trifluoroacetic acid (TFA) or a sodium acetate buffer (5 mM) at pH 8.0, which were heated to 55–60°C to improve peak resolution and purity.<sup>42,43</sup> Peptide identity,

verified by mass spectrometry and NMR,<sup>44</sup> had purity levels greater than 90%. Obtaining pure peptide as judged by NMR was critically important to maintaining the A $\beta$  peptide solubility.

Because the A $\beta$ (1–40) and A $\beta$ (1–42) peptides undergo time- and concentration-dependent aggregation in the acetonitrile–water used for HPLC purification,<sup>45</sup> the dry, purified peptides adopt different structures and aggregation states.<sup>36,37</sup> Depending on the commercial source, peptide batch, and the particular aggregation conditions, considerable discrepancies exist across different laboratories as well as within the same laboratory over time. In addition, numerous studies have established that the neurotoxicity and the kinetics of  $\beta$ -aggregation are directly related to assembly state in solution. Thus, direct solubilization of the A $\beta$  peptides in aqueous media should always be avoided, because it generates batch-dependent mixtures of aggregates and structures.

To disaggregate the A $\beta$  and generate monomeric random coil structure, we used a procedure recently developed in the Teplow laboratory<sup>38</sup> that involved predissolution of the peptide in dilute base solution. Our reasons for using this procedure, instead of our usual practice of A $\beta$  peptide predissolution in TFA and 1,1,1,3,3,3-hexafluoro-2-propanol solvents (HFIP),<sup>44</sup> are as follows: (1) after redissolution in aqueous buffer, the Teplow procedure is better at preventing the pH from inadvertently falling between 4 and 7, which is a pH range where aggregation is maximized,<sup>16</sup> and (2) the TFA–HFIP pretreatment method occasionally promoted partial Met35 oxidation of the A $\beta$ (1–42) peptide. Accordingly, the purified A $\beta$  peptides were predissolved in dilute NaOH solution (0.1 mL, 10 mM) in a 1:1 ratio (mg:mL) with sonication for 1 min.<sup>38</sup> The basic pH 10–11 solution of the A $\beta$  peptides (0.1 mL) was combined with a potassium phosphate buffered solution (0.4 mL, 5–20 mM, pH 7.2) in either D<sub>2</sub>O or H<sub>2</sub>O:D<sub>2</sub>O (9:1) with 0.50 mM perdeuterated ethylenediamine tetraacetic acid (Na<sub>2</sub>EDTA-*d*<sub>12</sub>), and 0.05 mM NaN<sub>3</sub>. The pH was carefully checked with a special pH electrode (Microelectrode) that fit inside the 5 mm NMR tube and, if needed, was carefully adjusted to pH 7.2 with dilute NaOD or TFA-*d*<sub>1</sub> solutions. The samples were prepared at 0.20–0.80 mM A $\beta$  concentrations, with the majority of NMR experiments done at 0.20–0.30 mM.

**Analytical Ultracentrifugation.** The sedimentation equilibrium experiments used a Beckman XL-A analytical ultracentrifuge at the University of Georgia, using procedures previously used with the A $\beta$  peptide with minor modifications.<sup>46</sup> The A $\beta$ (1–40)Met35<sup>red</sup> and A $\beta$ (1–42)Met35<sup>red</sup> samples were first prepared at the University of Georgia for NMR analysis (in D<sub>2</sub>O solvent), to ensure that the data were comparable to those obtained at Case Western Reserve University. Using the NMR sample, sedimentation equilibrium data were obtained at 30 000 rpm, 5 °C for 16 and 40 h (to ensure equilibrium) in three cells with 0.15, 0.30, and 0.45 mM A $\beta$  in D<sub>2</sub>O. The D<sub>2</sub>O solvent without peptide was used as optical reference at the wavelength of the measurements (275 nm). The ultracentrifugation data were fitted with optical absorbance instead of concentration by assuming that the sample obeys the Beer–Lambert law across the full range of absorbance. Data were fit to various self-association models by least-squares using the Beckman software, and goodness of fit was determined from the randomness of the residuals. The radial concentration for a single ideal species is

$$C_r = C_{r_0} \exp \left[ \frac{\omega^2}{2RT} M (1 - \bar{v}\rho) (r^2 - r_0^2) \right] \quad (1)$$

where  $C_r$  is the concentration at radius  $r$ ,  $C_{r_0}$  is the concentration at the reference radius  $r_0$ ,  $\omega$  is the angular velocity,  $\bar{v}$  is the partial specific volume of the peptide,  $R$  is the gas constant,  $T$  is the temperature in K,  $M$  is the monomer molecular weight, and  $\rho$  is the solvent density.

(39) Kontush, A. *Free Radical Biol. Med.* **2001**, *31*, 1120–1131.

(40) Shechter, Y. *J. Biol. Chem.* **1986**, *261*, 66–70.

(41) Stine, W. B., Jr.; Dahlgren, K. N.; Krafft, G. K.; LaDu, M. J. *J. Biol. Chem.* **2003**, *278*, 11612–11622.

(42) Boyes, B. E. *Efficient High Yield Reversed-Phase HPLC Separations of Amyloid Precursor Polypeptide C-Terminal Fragments*; 14th American Peptide Symposium, Columbus, OH, 1995.

(43) Neuhaus, E. B.; Menon, N. K.; Makula, R. A.; Przybyla, A. E. *Vydac Reversed-Phase Columns Aid in Purification of Recombinant Alzheimer's Proteins*. *Vydac Advances*; Vydac: Hesperia, CA, 1999; pp 4–5.

(44) Jao, S.-C.; Ma, K.; Talafous, J.; Orlando, R.; Zagorski, M. G. *Amyloid: Int. J. Exp. Clin. Invest.* **1997**, *4*, 240–252.

(45) Shen, C.-L.; Murphy, R. M. *Biophys. J.* **1995**, *69*, 640–651.

(46) Holzman, T. F.; Snyder, S. W. *Modern Analytical Ultracentrifugation*; Birkhauser: Boston, MA, 1994; pp 298–314.

For the A $\beta$ (1–40)Met35<sup>red</sup> peptide, the predicted monomeric molecular weight in D<sub>2</sub>O is 4377. A partial specific volume of 0.737 mL/g was estimated from the amino acid sequence and corrected for temperature. Apparent molecular weights were determined for each concentration data set. The lowest concentration (0.15 mM) gave a reasonable fit to a single ideal species with a fitted molecular weight of 4800  $\pm$  100 (the  $\pm$  corresponds to a 95% confidence interval). At higher concentrations, the calculated and fitted molecular weights were somewhat lower, 4700  $\pm$  100 for 0.30 mM and 4600  $\pm$  70 for 0.45 mM with poorer fits whose residuals suggested the presence of higher molecular weight species. More complicated association models were then tested, such as various monomer–multimer (n-mer) equilibria:

$$C_{r,\text{total}} = C_{\text{monomer},r_0} \exp[(1 - \bar{v}\rho)(r^2 - r_0^2)] + C_{n\text{-mer},r_0} \exp\left[\frac{\omega^2}{2RT}nM(1 - \bar{v}\rho)(r^2 - r_0^2)\right] \quad (2)$$

where  $C_{r,\text{total}}$  is the total concentration at radius  $r$ ,  $C_{\text{monomer},r_0}$  is the monomer concentration at radius  $r_0$ , and  $C_{n\text{-mer},r_0}$  is the n-mer concentration at radius  $r_0$ . The association constant is defined by  $K_a = C_{n\text{-mer}}/(C_{\text{monomer}})^n$ , and the dissociation constant is  $K_d = 1/K_a$ . Equation 2 assumes that the dimer and monomer have the same partial specific volume. A monomer–dimer model gives an acceptable fit at 0.15 mM, and the calculated monomer–dimer equilibrium constant was 1.9 mM. Data obtained at higher concentrations gave unsatisfactory fits, and attempts to fit these data using models with trimer and tetramer as possibilities were unsuccessful.

**NMR Spectroscopy.** All NMR spectra were acquired at 600 MHz using Varian Inova-600 spectrometers, with the exception of the 3D experiments that were acquired at 800 MHz with Varian Inova-800 and Bruker DRX-800 spectrometers. For all experiments, triple resonance 5 mm probes with actively shielded z-gradient coils were utilized. The NMR data were transferred to Octane-2 (Silicon Graphics) computer workstations, then processed and analyzed using the FELIX (Accelrys), XWINNMR (Bruker), NMRPIPE,<sup>47</sup> and PIPP<sup>48</sup> programs. The <sup>1</sup>H chemical shifts were referenced to an internal standard of sodium 3-(trimethylsilyl)propionate-2,2,3,3-*d*<sub>4</sub> (TSP), whereas the <sup>15</sup>N and <sup>13</sup>C chemical shifts were referenced indirectly relative to the internal standard 2,2-dimethyl-2-silapentane-5-sulfonic acid (DSS) using consensus ratios of 0.10132912 and 0.25144953, respectively.<sup>49</sup> The probe temperatures were calibrated using methanol and dimethyl sulfoxide solutions.

For the aging studies, A $\beta$ (1–40)Met35<sup>red</sup>, A $\beta$ (1–40)Met35<sup>ox</sup>, A $\beta$ (1–42)Met35<sup>red</sup>, and A $\beta$ (1–42)Met35<sup>ox</sup> peptide solutions (0.20 mM peptide, 10 mM potassium phosphate buffer, D<sub>2</sub>O, pH 7.2) were prepared in 5 mm NMR tubes and incubated in a thermostated water bath at 37.0 °C. At measured time intervals of heating, the samples were periodically withdrawn from the bath, and 1D NMR spectra were acquired for all samples using identical acquisition (37.0 °C, 2 s recycle delay, 64 scans, 32K complex data points) and processing parameters (exponential line broadening 2 Hz). The residual protium absorption of D<sub>2</sub>O (HDO) was suppressed by low-power irradiation during the recycle delay. To ensure that the pH was kept constant throughout the incubation, the pH was measured at the beginning and end of all experiments, and generally these values agreed  $\pm$ 0.1 pH unit. For the 2D and 3D experiments conducted in H<sub>2</sub>O solvent, pulsed field gradients sequences (such as the WATERGATE) were employed to suppress the solvent resonance.<sup>50</sup> The 2D NOESY and clean-TOCSY<sup>51</sup> were acquired in the States mode with 2 s recycle delay and mixing times of 150–250 and 30–80 ms,

respectively. The acquired data sizes were generally 512  $\times$  4096 complex points in the  $t_1$  and  $t_2$  time-domains, which were zero-filled to 4096  $\times$  4096 real points in the  $F_1$  and  $F_2$  dimensions. The <sup>3</sup>J<sub>NH- $\alpha$ H coupling constants were obtained from a 2D DQF-COSY spectrum, which was corrected for NH line widths contributions and zero-filled twice in the  $F_2$  dimension to increase the digital resolution to 0.85 Hz/pt.<sup>52</sup> For determination of the NH temperature coefficients ( $-\Delta\delta/\Delta T$ , ppb), the amide-NH chemical shifts were obtained from NOESY and TOCSY spectra acquired between 2.0 and 20.0 °C (0.20 mM peptide concentration, pH 7.2), from which the coefficients were taken as the slopes from least-squares computer fitted lines of the chemical shifts against temperature. Essentially all curves were linear, with correlation coefficients in the range 0.995–1.00. The 2D <sup>1</sup>H–<sup>15</sup>N HSQC experiments were recorded (on average) with 32 scans, 2048 complex points, and the transmitter placed on the water signal.<sup>53</sup> The sweep widths were 6373.5 and 2000.0 Hz in the  $F_1$  and  $F_2$  dimensions, respectively. The 3D experiments, which included the <sup>15</sup>N-edited NOESY-HSQC, HNHA, and HNCACB, were acquired in States-TPPI mode,<sup>54</sup> and typically with 32 ( $t_1$ )  $\times$  180 ( $t_2$ )  $\times$  2048 ( $t_3$ ) complex points, which were zero-filled to provide matrices with 64  $\times$  512  $\times$  2048 real data points. Usually four scans were acquired for each increment, and the total acquisition times were 29–40 h. The chemical shift indices of the <sup>1</sup>H $\alpha$ , <sup>13</sup>C $\alpha$ , and <sup>13</sup>C $\beta$  were generated using the CSI program (Protein Engineering Network of Centres of Excellence, University of Alberta).<sup>49</sup></sub>

**Diffusion Measurements.** The diffusion coefficients ( $D$ ) were obtained at 600 MHz using the NMR PFG-water-sLED pulse sequence.<sup>55</sup> For accuracy, the  $D$  values for standard proteins (lysozyme and ubiquitin) were first measured and found to be in almost complete agreement ( $\pm 0.02 \times 10^{-6}$  cm<sup>2</sup> s<sup>-1</sup>) with the literature values, hence establishing the validity in our experimental approach. Data accumulation involved acquiring an array of 15 spectra (32 scans each, 5 s recycle delay) with different gradient strengths ( $g$ ) varying from 0.3 to 30 G/cm.

The NMR signal intensities are related to the  $D$  value according to the following relationship:

$$R = \exp[-\gamma g \delta]^2 D(\Delta - \delta/3)]$$

where  $R$  is the ratio of intensities for a resonance with the gradient on ( $I$ ) to that with the gradient off ( $I_0$ ),  $\gamma$  is the gyromagnetic ratio of <sup>1</sup>H ( $2.675 \times 10^4$  G<sup>-1</sup> s<sup>-1</sup>),  $g$  and  $\delta$  are the magnitude and duration of the gradient pulses, respectively, and  $\Delta$  is the time between the gradient pulses. For our studies, the following parameters were used:  $\delta = 5.5$  ms,  $g = 0.3$ –30 G/cm,  $\Delta = 220$ –320 ms, and a longitudinal eddy-current delay of 40 ms. The upfield methyl signals (0.73–1.52 ppm) and downfield aromatic signals (6.74–8.66 ppm) were integrated to provide the signal intensities ( $I$  and  $I_0$ ), and these data were approximated as single, exponentially decaying curves [plots of  $R$  vs ( $g^2$ )] using averaged fitting values obtained from the Origin program (Microcal).

## Results

**Aggregation State.** To overcome problems related to time-dependent aggregation of the A $\beta$  peptides, all pre-aggregated (seed) peptide material was carefully removed from the samples prior to NMR analysis (see Experimental Procedures). The A $\beta$  peptide solutions (up to 0.80 mM) were stable for several days at pH 7.2 and 5 °C, with no precipitation or other spectral changes detected by NMR. In addition, no concentration-dependent changes in chemical shifts and line widths were seen, consistent with the presence of intact, nondegraded monomeric peptide.

(47) Delaglio, F.; Grzesiek, S.; Vuister, G. W.; Zhu, G.; Pfeifer, J.; Bax, A. J. *Biomol. NMR* **1995**, *6*, 277–293.

(48) Garrett, D. S.; Powers, R.; Gronenborn, A. M.; Clore, G. M. *J. Magn. Res.* **1991**, *95*, 214–220.

(49) Wishart, D. S.; Nip, A. M. *Biochem. Cell Biol.* **1998**, *76*, 153–163.

(50) Kay, L. E. *Prog. Biophys. Mol. Biol.* **1995**, *63*, 277–299.

(51) Griesinger, C.; Otting, G.; Wüthrich, K.; Ernst, R. R. *J. Am. Chem. Soc.* **1988**, *110*, 7870–7872.

(52) Wüthrich, K. *NMR of Proteins and Nucleic Acids*; Wiley: New York, 1986.

(53) Bax, A.; Grzesiek, S. *Acc. Chem. Res.* **1993**, *26*, 131–138.

(54) Sattler, M. S.; Beunink, J.; Griesinger, C. *Prog. Nucl. Magn. Reson. Spectrosc.* **1999**, *34*, 93–158.

(55) Altieri, A. S.; Hinton, D. P.; Byrd, R. A. *J. Am. Chem. Soc.* **1995**, *117*, 7566–7567.

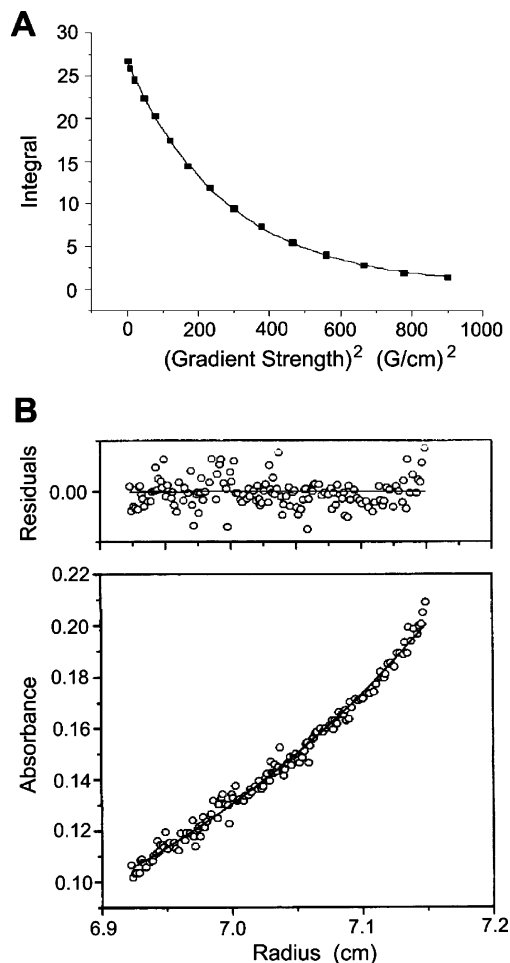


**Figure 1.** (A) Pulse-field gradient diffusion experiments of the  $A\beta(1-40)$  in buffered  $D_2O$  (0.30 mM, 20 °C, pH 7.2), with the exponential decay curve fitting of the spectral integrals in the aliphatic region with increasing gradient strength. The experiment could be reproduced three times, and the precision of the integral data is  $\pm 0.50$ . The diffusion coefficient was calculated from the exponential decay fitting ( $(12.0 \pm 0.35) \times 10^{-7} \text{ cm}^2 \text{ s}^{-1}$ ). (B) Sedimentation equilibrium of the  $A\beta(1-40)$  at 0.15 mM and 40 h incubation at 5 °C. These data gave a reasonable fit to a single ideal species with a molecular weight of  $4756 \pm 111$ , with the lower figure showing the absorbance at 275 nm versus the distance from the center of rotation. The line drawn through the points gives the expected absorbance, assuming a monomer-dimer equilibrium. The upper figure shows the residuals calculated from the actual absorbance values and those represented by the line.

To confirm the  $A\beta$  aggregation state, NMR diffusion and sedimentation equilibrium experiments were undertaken. The translational diffusion coefficient ( $D$ ) provides reliable information about the molecular sizes and the apparent molecular weights of proteins, and in some cases can also provide fractional populations of different aggregation states.<sup>56</sup> The  $D$  values were obtained by monitoring signal losses in the upfield methyl and downfield aromatic spectral regions as a function of gradient strength (Figure 1A), and the calculated  $D$  values at peptide concentrations of 0.30 mM were  $(12.0 \pm 0.35) \times 10^{-7} \text{ cm}^2 \text{ s}^{-1}$ . Using the Stokes-Einstein equation, the molecular hydrodynamic radius was evaluated, and this was consistent with either a monomeric extended, or a folded, compact dimeric structure. If present, the dimeric structure would have to be completely symmetric (due to the presence of one set of NMR

resonances for each amino acid residue) or result from a rapid exchange of monomers within a dimer.

The sedimentation equilibrium measurements were carried out with an analytical ultracentrifuge using three peptide concentrations (0.15, 0.30, and 0.45 mM). To ensure that they were consistent with the other samples used for spectral assignments, the samples were first inspected by NMR. For the  $A\beta(1-40)\text{Met35}^{\text{red}}$ , the lowest concentration afforded a reasonably good fit to a single ideal species with a fitted molecular weight of  $4800 \pm 100$ , which provided an acceptable monomer-dimer equilibrium constant of 1.9 mM (Figure 1B). At the higher concentrations, somewhat lower calculated, fitted molecular weights ( $4700 \pm 100$  and  $4600 \pm 70$ ) were obtained, with poorer fits whose residual profiles suggested that higher molecular weight species were present. Attempts to fit these latter data using models with trimer and tetramers as possibilities were unsuccessful. These results showed that under the solution conditions employed, the  $A\beta$  exists predominantly (>90%) as a monomer, even though higher molecular weight species are also present, some of which are probably larger than tetramers.

In summary, the lack of any concentration-dependent NMR chemical shift changes, together with the NMR diffusion and sedimentation equilibrium measurements, all establish that the  $A\beta$  peptides are predominantly extended and monomeric (>90%) over the concentration range 0.15–0.80 mM. These results agree with recent sedimentation velocity measurements of the  $A\beta$  peptide from another laboratory (Jeff Kelly and Hillal Lashuel, personal communication). The discrepancies with previous reports of stable  $A\beta(1-40)$  and  $A\beta(1-42)$  dimers<sup>57,58</sup> that may be at equilibrium with the monomers<sup>59</sup> may be that their techniques were detecting the higher ordered aggregates, which in our case represent less than 10% and are not seen by NMR. Another possibility may be due to slight variations in the sample preparation protocols, the analytical procedures employed, or possibly the temperature used to assess aggregation (to prevent aggregation, our studies were done without salt and at lower temperatures<sup>33,60,61</sup>). Additionally, our sample preparation protocol ensures that the  $A\beta(1-40)$  and  $A\beta(1-42)$  peptides are completely disaggregated before dissolution in aqueous solution at pH 7.2 (see Experimental Procedures).

**NMR Chemical Shift Assignments.** For completing the NMR assignments, it is imperative that a single (stable) structure predominates, giving reproducible data over several days, as required for long 2D and 3D NMR data acquisitions. At concentrations of 0.20–0.80 mM, the  $A\beta(1-40)\text{Met35}^{\text{red}}$ ,  $A\beta(1-40)\text{Met35}^{\text{ox}}$ , and  $A\beta(1-42)\text{Met35}^{\text{ox}}$  peptides remained soluble and monomeric in aqueous solution at pH 7.2 and 0–20 °C, with no detectable changes in chemical shifts, line widths, or loss of signal/noise. By contrast, at comparable concentrations, the  $A\beta(1-42)\text{Met35}^{\text{red}}$  remained soluble only at temperatures  $\leq 5$  °C. Thus, to maintain a single set of solution conditions and overcome the insolubility issues with the  $A\beta(1-$

- (57) Roher, A. E.; Chaney, M. O.; Kuo, Y.-M.; Webster, S. D.; Stine, W. B.; Haverkamp, L. J.; Woods, A. S.; Cotter, R. J.; Tuohy, J. M.; Krafft, G. A.; Bonnell, B. S.; Emmerling, M. R. *J. Biol. Chem.* **1996**, *271*, 20631–20635.  
 (58) Garzon-Rodriguez, W.; Sepulveda-Becerra, M.; Milton, S.; Glabe, C. G. *J. Biol. Chem.* **1997**, *272*, 21037–21044.  
 (59) Pallitto, M. M.; Murphy, R. M. *Biophys. J.* **2001**, *81*, 1805–1822.  
 (60) Snyder, S. W.; Lador, U. S.; Wade, W. S.; Wang, G. T.; Barrett, L. W.; Matayoshi, E. D.; Huffaker, H. J.; Krafft, G. A.; Holzman, T. F. *Biophys. J.* **1994**, *67*, 1216–1228.  
 (61) Kusumoto, Y.; Lomakin, A.; Teplow, D. B.; Benedek, G. B. *Proc. Natl. Acad. Sci. U.S.A.* **1998**, *95*, 12277–12282.

(56) Mayo, K. H.; Ilyina, E. *Protein Sci.* **1998**, *7*, 358–368.

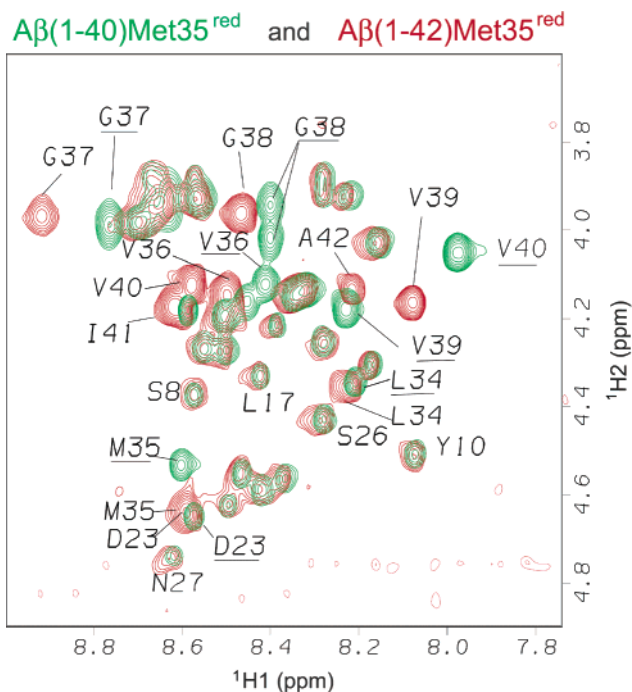


**Figure 2.** Expanded and overlaid TOCSY contour plots (NH–H $\alpha$  region) for the A $\beta$ (1–40)Met35<sup>red</sup> (green peaks) and A $\beta$ (1–42)Met35<sup>red</sup> (red peaks) peptides. The two TOCSY spectra (600 MHz) were obtained at 5 °C using 0.80 mM samples in buffered (5 mM sodium phosphate, pH 7.2) aqueous solution (9:1, H<sub>2</sub>O:D<sub>2</sub>O) with 0.50 mM Na<sub>2</sub>EDTA and 0.05 mM NaN<sub>3</sub>. The cross-peaks represent intraresidue couplings between the H $\alpha$  and NH. Peaks displaying apparent chemical shift differences between the A $\beta$ (1–40)Met35<sup>red</sup> and A $\beta$ (1–42)Met35<sup>red</sup> are underlined for the former peptide and reside within the Met35–Val40 region. Besides the shift differences, separate  $\alpha$ H signals were seen for the Gly38 of A $\beta$ (1–40)Met35<sup>red</sup> (ABX spin system) but not for the A $\beta$ (1–42)Met35<sup>red</sup> (A<sub>2</sub>X spin system).

42)Met35<sup>red</sup>, the NMR experiments for the four peptides were conducted at 5 °C. The relationship of increased A $\beta$  aggregation rates and temperature agrees with earlier reports.<sup>33,61</sup>

The complete <sup>1</sup>H NMR spectra of the A $\beta$ (1–40)Met35<sup>red</sup>, A $\beta$ (1–40)Met35<sup>ox</sup>, A $\beta$ (1–42)Met35<sup>red</sup>, and A $\beta$ (1–42)Met35<sup>ox</sup> peptides were assigned with the use of standard homonuclear methodology.<sup>52</sup> Shown in Figure 2 are superimposed TOCSY spectra of the fingerprint (NH–H $\alpha$ ) region of the A $\beta$ (1–40)Met35<sup>red</sup> and A $\beta$ (1–42)Met35<sup>red</sup> peptides. With the exception of minor shift differences (0.1 ppm) for the Met35, the majority of the <sup>1</sup>H $\alpha$  chemical shifts are identical for the two peptides, indicative of similar secondary structures.<sup>49</sup> However, for residues located at the hydrophobic C-terminus (Val36–Gly37–Gly38–Val39–Val40), several chemical shift differences were apparent, with the NH of the A $\beta$ (1–42)Met35<sup>red</sup> peptide appearing at slightly higher field by approximately 0.2–0.3 ppm. For the A $\beta$ (1–40)Met35<sup>ox</sup> and A $\beta$ (1–42)Met35<sup>ox</sup> peptides, two sets of <sup>1</sup>H resonances were seen for the two diastereomeric Met35<sup>ox</sup> side chains, in accordance with previous studies.<sup>24,34</sup>

The NMR assignment of the <sup>15</sup>N atoms was accomplished using data from two 3D NMR experiments (HNHA and <sup>15</sup>N-edited NOESY-HSQC) and well-established assignment protocols.<sup>54</sup> With uniformly <sup>15</sup>N-labeled A $\beta$  peptides, the backbone <sup>15</sup>N chemical shifts were assigned using HNHA data, which provides through-bond connectivity among intraresidue <sup>15</sup>NH, <sup>15</sup>N, and <sup>1</sup>H $\alpha$  atoms. The assignment task was fairly straightforward, because of the knowledge of the <sup>1</sup>H $\alpha$  and NH chemical shifts obtained from the homonuclear <sup>1</sup>H NMR data. The few

unresolved assignments, as well as the side-chain Gln15 and Asn27 <sup>15</sup>N atoms, were located with the <sup>15</sup>N-edited NOESY-HSQC. Figure 3 presents two 2D HSQC spectra for the 40- and 42-residue peptides, with spectral superimposition of the A $\beta$ (1–40)Met35<sup>red</sup> and A $\beta$ (1–40)Met35<sup>ox</sup>, and also the A $\beta$ (1–42)Met35<sup>red</sup> and A $\beta$ (1–42)Met35<sup>ox</sup>. The narrow NH chemical shift dispersion suggests that the four peptides adopt predominantly random extended chain structures. The A $\beta$ (1–40)Met35<sup>red</sup> and A $\beta$ (1–40)Met35<sup>ox</sup> have different NH chemical shifts for the three amino acid residues (Leu34–Met35–Val36) (Figure 3A), while the A $\beta$ (1–42)Met35<sup>red</sup> and A $\beta$ (1–42)Met35<sup>ox</sup> show different NH chemical shifts for six residues (Leu34–Met35–Val36–Gly37–Gly38–Val39) (Figure 3B). The NH shifts are downfield for A $\beta$ (1–42)Met35<sup>ox</sup> relative to the A $\beta$ (1–42)Met35<sup>red</sup>, except for Gly37–Gly38 that are shifted upfield.

With uniformly <sup>13</sup>C- and <sup>15</sup>N-doubly labeled A $\beta$  peptides, the backbone <sup>13</sup>C $\alpha$  and <sup>13</sup>C $\beta$  chemical shifts were identified with HNCACB spectral data. The HNCACB experiment correlates the <sup>15</sup>NH and <sup>15</sup>N resonances with the <sup>13</sup>C $\alpha$  and <sup>13</sup>C $\beta$  of both the same amino acid (intraresidue connectivity) and the preceding amino acid (interresidue connectivity).<sup>54</sup> The <sup>13</sup>C assignments were utilized for secondary structure determination, as is discussed in the following section.

#### Secondary Structure Determination from the NMR Data.

The secondary structures were arrived at from interpretation of the interresidue NOE connectivities among the backbone NH, <sup>1</sup>H $\alpha$ , and <sup>1</sup>H $\beta$  atoms, combined with analysis of the <sup>1</sup>H $\alpha$ , <sup>13</sup>C $\alpha$ , and <sup>13</sup>C $\beta$  chemical shifts.<sup>52</sup> Representative NOE connectivities for the A $\beta$ (1–40)Met35<sup>red</sup> and A $\beta$ (1–40)Met35<sup>ox</sup> peptides are displayed in Figure 4, and similar NOE patterns were observed for the A $\beta$ (1–42)Met35<sup>red</sup> and A $\beta$ (1–42)Met35<sup>ox</sup> (data not shown). Overall, more NOEs were seen with the peptides containing Met35<sup>red</sup>, including sequential short-range (adjacent amino acid residues) such as between the <sup>1</sup>H $\alpha$  and the NH [listed as  $\alpha$ N(*i*,*i*+1)], as well as weaker-sized NOEs between the adjacent NHs [listed as NN(*i*,*i*+1)]. Medium-range NOEs (nonadjacent residues), such as the  $\alpha$ N(*i*,*i*+2) between the  $\alpha$ H of Phe20 and the NH of Glu22, were seen only in certain peptide regions. For the A $\beta$ (1–40)Met35<sup>red</sup>,  $\alpha$ N(*i*,*i*+2) NOEs were seen within the Asp7–Glu11, Phe20–Ser26, and Gly29–Ile31 regions, plus one  $\alpha$ N(*i*,*i*+3) NOE between Asp23 and Ser26. With the A $\beta$ (1–40)Met35<sup>ox</sup> peptide,  $\alpha$ N(*i*,*i*+2) NOEs were seen only in the Phe20–Val24 and Gly29–Ile31 regions, and no  $\alpha$ N(*i*,*i*+3) NOEs were detected.

For all peptides, the residue-specific ratios of the  $\alpha$ N(*i*,*i*+1)/NN(*i*,*i*+1) intensities indicate a population weighted heavily toward random extended chain structure.<sup>62</sup> The average values of the *J*-coupling constants between the <sup>1</sup>H $\alpha$  and NH protons (7–8 Hz) are also consistent with these interpretations, although some values were slightly larger (8–9 Hz), suggesting the possibility of localized  $\beta$ -strand structure in some regions. We did not observe any intermolecular NOEs that would be present from aggregation, consistent with monomeric structure as determined from sedimentation equilibrium measurements. The lack of sufficient medium-range and long-range NOEs (greater than four residues apart) suggests that, under the present solution conditions, the A $\beta$  peptides do not fold into well-defined tertiary

(62) Fiebig, K. M.; Schwalbe, H.; Buck, M.; Smith, L. J.; Dobson, C. M. J. *Phys. Chem.* **1996**, *100*, 2661–2666.

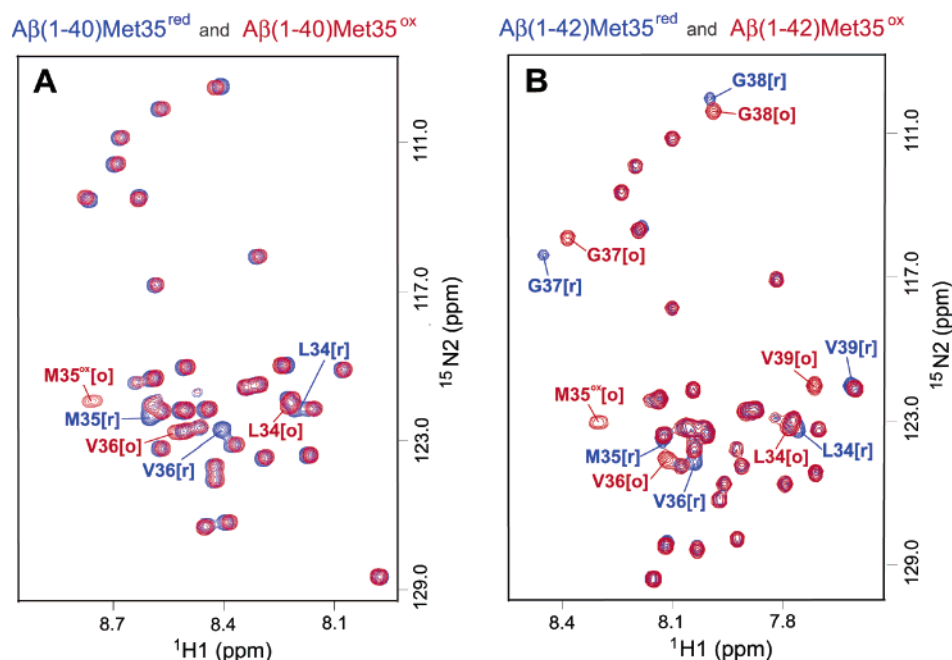


**Figure 3.** The overlaid  $^1\text{H}$ – $^{15}\text{N}$  HSQC spectra of recombinant  $^{15}\text{N}$ -labeled  $\text{A}\beta$  peptides (0.25 mM) in 9:1  $\text{H}_2\text{O}:\text{D}_2\text{O}$ , pH 7.2,  $5^\circ\text{C}$ . (A)  $\text{A}\beta(1-40)\text{Met}35^{\text{red}}$  (blue) and  $\text{A}\beta(1-40)\text{Met}35^{\text{ox}}$  (red), and (B)  $\text{A}\beta(1-42)\text{Met}35^{\text{red}}$  (blue) and  $\text{A}\beta(1-42)\text{Met}35^{\text{ox}}$  (red). The  $^{15}\text{NH}$  peaks showing different chemical shifts between the  $\text{Met}35^{\text{ox}}$  and  $\text{Met}35^{\text{red}}$  peptides are labeled. These data show that oxidation of the  $\text{Met}35$  side chain promotes shift changes of the  $\text{Leu}34$ – $\text{Met}35$ – $\text{Val}36$  in  $\text{A}\beta(1-40)$  and the  $\text{Leu}34$ – $\text{Met}35$ – $\text{Val}36$ – $\text{Gly}37$ – $\text{Gly}38$ – $\text{Val}39$  in  $\text{A}\beta(1-42)$ .

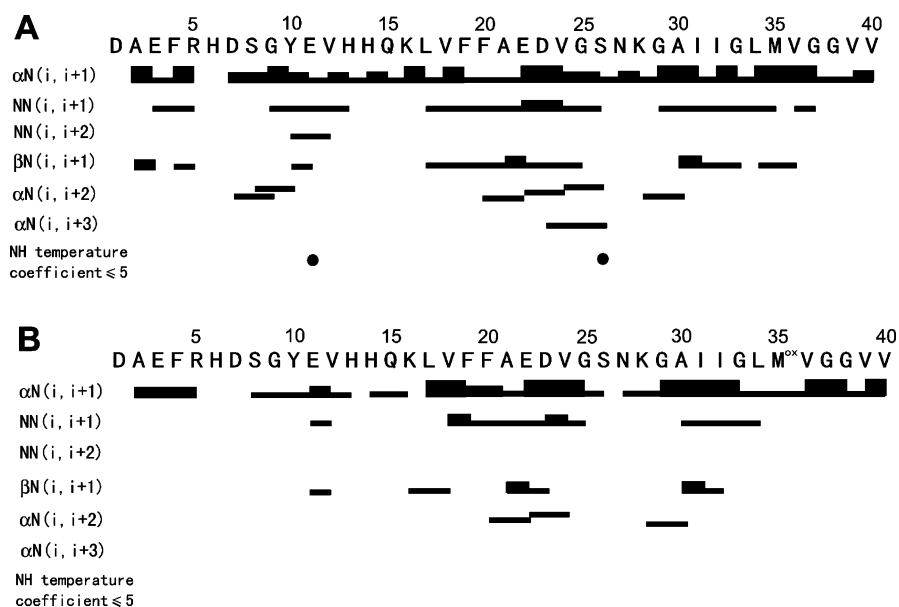


**Figure 4.** Summary of the NH temperature coefficient and observed interresidue sequential NOE data among the backbone NH,  $\text{H}\alpha$ , and  $\text{H}\beta$  atoms for the (A)  $\text{A}\beta(1-40)\text{Met}35^{\text{red}}$  and (B)  $\text{A}\beta(1-40)\text{Met}35^{\text{ox}}$  peptides. The NOE intensities are reflected by the thickness of the lines.

structures. For these reasons and the lack of sufficient input constraints, we did not attempt to solve a tertiary structure using reconstruction algorithms.

Analysis of the solvent exposure and strength of the NH backbone groups was done by hydrogen to deuterium exchange ( $\text{NH} \rightarrow \text{ND}$ ) and measurement of the NH temperature coefficients. For all peptides, the  $\text{NH} \rightarrow \text{ND}$  exchange rates were extremely rapid in  $\text{D}_2\text{O}$  solvent at  $5^\circ\text{C}$  and not amenable to rate analysis. With the temperature coefficients, only the NH groups of  $\text{Glu}11$  and  $\text{Ser}26$  of the  $\text{A}\beta(1-40)\text{Met}35^{\text{red}}$  were less than 5, indicative of weak backbone hydrogen bonding (Figure 4). These results, along with the presence of medium-range

NOEs (Figure 4), suggest some proclivity toward turn- or bendlike structures in the  $\text{Asp}7$ – $\text{Glu}11$  and  $\text{Phe}20$ – $\text{Ser}26$  regions for the peptides containing  $\text{Met}35^{\text{red}}$ .

To further explore the possibility of residual local structure, estimation of the secondary structures was obtained with the chemical shift indices of the  $^1\text{H}\alpha$ ,  $^{13}\text{C}\alpha$ , and  $^{13}\text{C}\beta$  atoms (Figure 5).<sup>49</sup> In the CSI analysis, an index of  $-1$ ,  $0$ , or  $1$  corresponds to  $\alpha$ -helix, random coil, or  $\beta$ -strand, respectively, and is assigned to each residue on the basis of the chemical shift deviation relative to the statistic random coil values. The observation of three or more contiguous residues with similar CSI values usually is indicative of a particular secondary structure. With

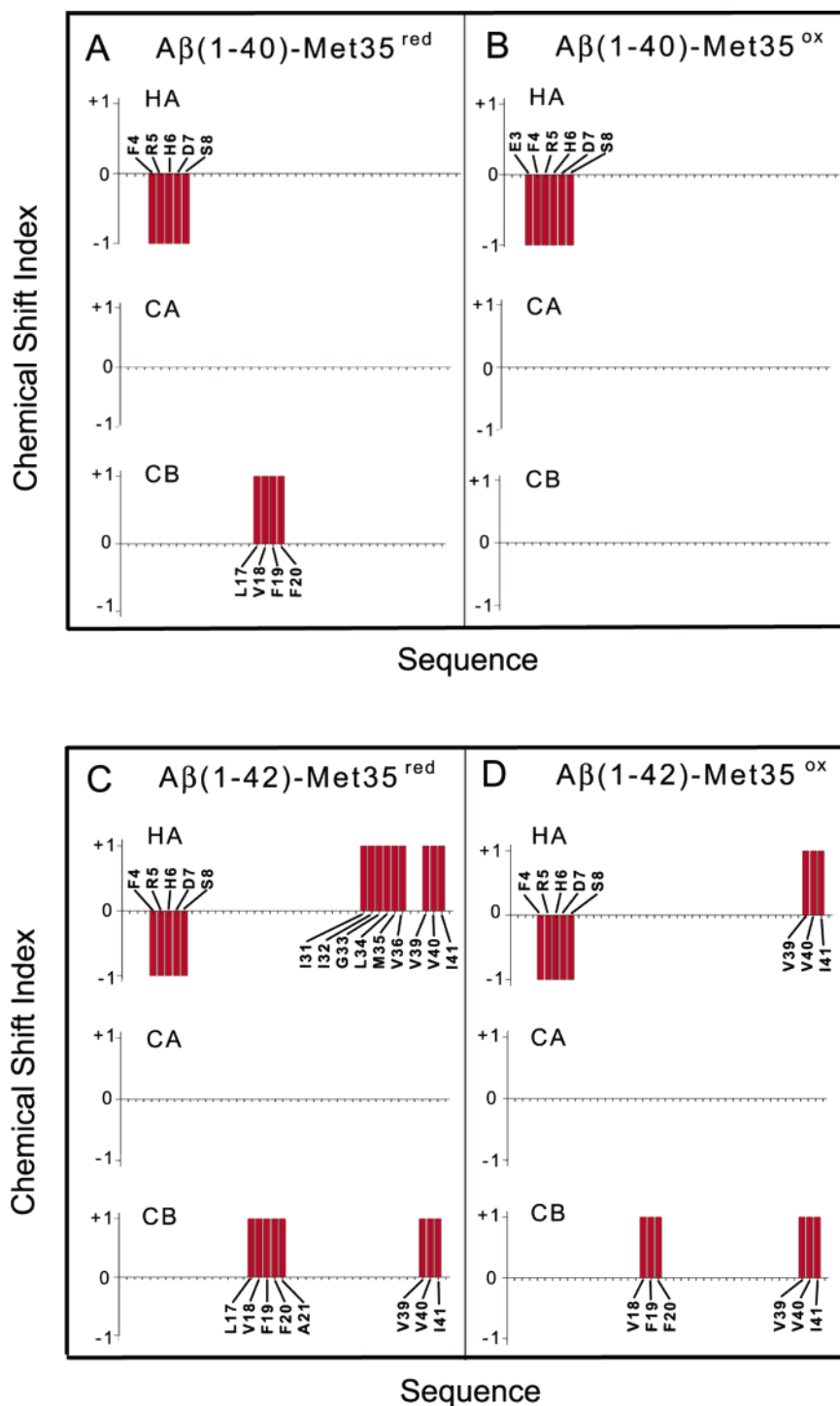


**Figure 5.** The  $^1\text{H}\alpha$ ,  $^{13}\text{C}\alpha$ , and  $^{13}\text{C}\beta$  chemical shift indices of the (A)  $A\beta(1-40)\text{Met35}^{\text{red}}$ , (B)  $A\beta(1-40)\text{Met35}^{\text{ox}}$ , (C)  $A\beta(1-42)\text{Met35}^{\text{red}}$ , and (D)  $A\beta(1-40)\text{Met35}^{\text{ox}}$  peptides. Indices of  $-1$ ,  $0$ , and  $1$  correspond to  $\alpha$ -helix, random coil, and  $\beta$ -strand structures, respectively. The marks along the x-axis represent the primary amino acid sequence, and residues showing indices of  $-1$  and  $1$  are labeled. The zero CSI values for the  $^{13}\text{C}\alpha$  and the greater sensitivity of the  $^{13}\text{C}\beta$  and  $^1\text{H}\alpha$  in detecting  $\beta$ -strand structure is consistent with the order  $^{13}\text{C}\alpha > ^{13}\text{C}\beta > ^1\text{H}\alpha > ^{15}\text{N} > ^1\text{H}^{\text{N}}$  for distinguishing  $\alpha$ -helix from random coil and  $^1\text{H}\alpha > ^{13}\text{C}\beta > ^1\text{H}^{\text{N}} \approx ^{13}\text{C}\alpha \approx ^{13}\text{C}^{\prime} \approx ^{15}\text{N}$  for distinguishing  $\beta$ -strand from random coil.<sup>63</sup>

the four  $A\beta$  peptides, the majority of the CSI values are zero, demonstrating that they adopt predominantly random structures, consistent with the interpretation using the NOE data. However, based on the  $^1\text{H}\alpha$  CSI, the N-terminal residues (Phe4–Ser8) show tendency toward  $\alpha$ -helical structure, although the presence of a stable  $\alpha$ -helix is not supported from the NOE and NH exchange data. CSI differences between the  $\text{Met35}^{\text{red}}$  and  $\text{Met35}^{\text{ox}}$  peptides are apparent, in that the reduced forms favored

$\beta$ -strand structures in specific regions. For example, the  $^{13}\text{C}\beta$  CSI shows  $\beta$ -strand structure at Leu17–Val18–Phe19–Phe20 for the  $A\beta(1-40)\text{Met35}^{\text{red}}$  but not for the  $A\beta(1-40)\text{Met35}^{\text{ox}}$  (Figure 5A and B). With the  $A\beta(1-42)\text{Met35}^{\text{red}}$ , the  $^{13}\text{C}\beta$  CSI shows  $\beta$ -strand structure at the Leu17–Val18–Phe19–Phe20–Ala21, while with the  $A\beta(1-42)\text{Met35}^{\text{ox}}$  peptide, it is at Val18–Phe19–Phe20 (Figure 5C and D). Larger differences were observed from the  $^1\text{H}\alpha$  CSI at the hydrophobic C-terminal

segment. For the  $A\beta(1-42)\text{-Met35}^{\text{red}}$ ,  $\beta$ -strand structure was observed for Ile31–Val36, and both 42-residue peptides favor  $\beta$ -strand structure at Val39–Val40–Ile41. By contrast, neither of the 40-residue peptides show tendency for  $\beta$ -strand structure at the hydrophobic C-terminus (Gly29–Val40), suggesting that this region may not be a driving force for  $\beta$ -aggregation with the  $A\beta(1-40)$ . The zero CSI values for the  $^{13}\text{C}\alpha$  and the greater sensitivity of the  $^{13}\text{C}\beta$  and  $^1\text{H}\alpha$  in detecting  $\beta$ -strand structure is consistent with probability-based secondary structure estimations of other proteins.<sup>63</sup> Thus, the reliability of CSI predictions follows the order  $^{13}\text{C}\alpha > ^{13}\text{C}' > ^1\text{H}\alpha > ^{13}\text{C}\beta > ^{15}\text{N} > ^1\text{H}^{\text{N}}$  for distinguishing  $\alpha$ -helix from random coil and  $^1\text{H}\alpha > ^{13}\text{C}\beta > ^1\text{H}^{\text{N}} \approx ^{13}\text{C}\alpha \approx ^{13}\text{C}' \approx ^{15}\text{N}$  for distinguishing  $\beta$ -strand from random coil.<sup>63</sup> Altogether, these results indicate that the  $A\beta$  peptides adopt predominantly random and  $\beta$ -strand conformations and that the Met35 oxidation reduces the  $\beta$ -strand forming propensities at both the C-terminal and the central hydrophobic segments.

**Influence of the Met35 Oxidation State on the Side-Chain Chemical Shifts.** In general, the Met35 oxidation state did not significantly alter the side-chain NMR chemical shifts, with the exception of the histidine 2H aromatic signals. Graphical depictions of the 2H and 4H chemical shifts for the three histidines (His6, His13, His14) and other aromatic residues (Tyr10, Phe4, Phe19, Phe20) are shown in Figure 6A and B for the two  $A\beta(1-40)$  peptides, and the two  $A\beta(1-42)$  peptides, respectively. The difference map graphs (lower sections) emphasize that oxidation of the Met35 promotes upfield chemical shifts for the histidine 2H signals. This effect is more pronounced for the  $A\beta(1-40)$  (Figure 6A), where upfield shifts of 0.22, 0.28, and 0.30 ppm are seen for His6, His14, and His13, as compared to 0.06, 0.07, and 0.07 ppm for the  $A\beta(1-42)\text{-Met35}$  peptide (Figure 6B). By comparison, the histidine 4H and other aromatic signals (Tyr10, Phe4, Phe19, Phe20) show negligible chemical shift changes ( $<0.05$  ppm). These results are remarkable given the extraneous location of the Met35 with the His6, His13, and His14 in the primary sequence.

**Aging Studies.** As discussed in the previous sections, to prevent aggregation, maintain peptide solubility, and obtain reproducible NMR data for a period of several days, the assignments were conducted with  $A\beta$  peptide solutions of low ionic strength, kept at low temperatures ( $\leq 5$  °C). It is well known that temperature is an important environmental variable that affects  $\beta$ -aggregation and the related conformational conversions (random  $\rightarrow$   $\beta$ -strand).<sup>16,33,61</sup> To explore these conformational changes in greater detail, aggregating  $A\beta$  peptide solutions were monitored by 1D NMR spectroscopy at specific time intervals during incubation at higher temperature (37 °C instead of 5 °C). In brief, three major spectral changes were observed: (1) in the aromatic region (6.8–7.8 ppm), the 2H signals for the three histidines (His6, His13, His14) progressively moved upfield, (2) peak movements were present in the 2.60–3.00 ppm region, and (3) there was a progressive loss in signal/noise.

Graphical plots showing the gradual changes of the histidine 2H chemical shifts with incubation time are shown in Figure 7A and B for the  $A\beta(1-40)$  and  $A\beta(1-42)$  peptides, respectively. To facilitate comparison between the  $\text{Met35}^{\text{red}}$  and  $\text{Met35}^{\text{ox}}$  peptides, the graphs contain two y-axes: the left y-axis

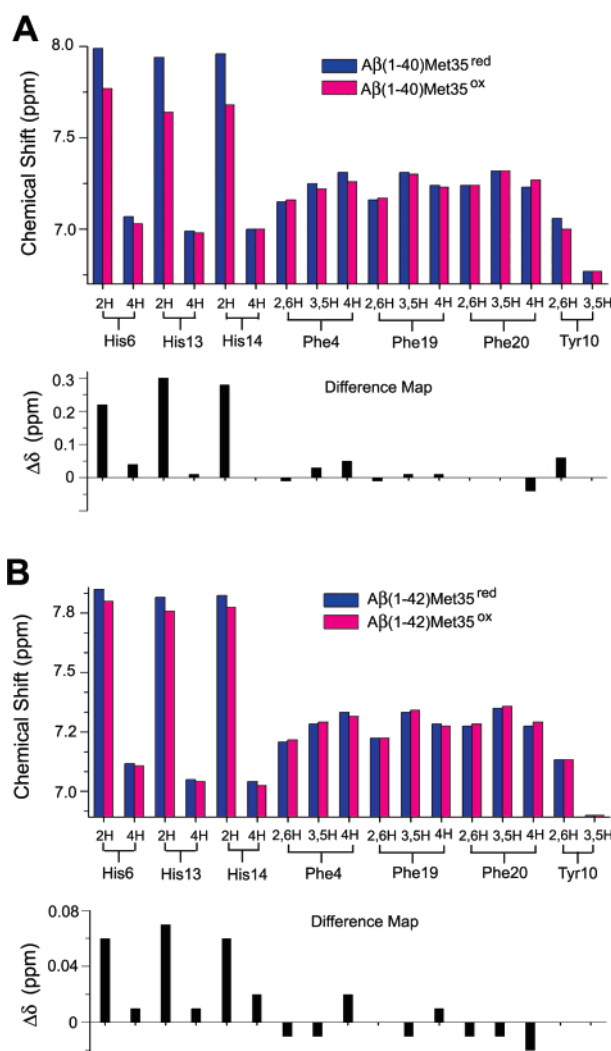


**Figure 6.** Bar graph showing the aromatic ring  $^1\text{H}\alpha$  chemical shifts for the (A)  $A\beta(1-40)\text{Met35}^{\text{red}}$  (blue) and  $A\beta(1-40)\text{Met35}^{\text{ox}}$  (red) and (B)  $A\beta(1-42)\text{Met35}^{\text{red}}$  (blue) and  $A\beta(1-42)\text{Met35}^{\text{ox}}$  (red) peptides. The difference map represents the chemical shift difference between the  $\text{Met35}^{\text{red}}$  and  $\text{Met35}^{\text{ox}}$ . These data establish that the Met35 oxidation state exerts a large effect on the histidine 2H chemical shift in the  $A\beta(1-40)$  peptide.

represents the histidine 2H chemical shift for  $\text{Met35}^{\text{red}}$  peptides, while the right y-axis represents the histidine 2H for the  $\text{Met35}^{\text{ox}}$  peptides. These data establish the Met35 oxidation hinders upfield movement of these signals and that this effect is more pronounced with the  $A\beta(1-40)$  peptide. The  $A\beta(1-40)\text{Met35}^{\text{ox}}$  and  $A\beta(1-42)\text{Met35}^{\text{ox}}$  peptides showed only minor movements ( $>0.01$  ppm) of the histidine 2H and only minor losses in signal/noise throughout incubation at 37 °C. For the  $A\beta(1-40)\text{Met35}^{\text{red}}$ , the total upfield shifts observed after 180 h incubation are 0.03, 0.02, and 0.02 ppm for His6, His13, and His14, respectively, whereas for the  $A\beta(1-42)\text{Met35}^{\text{red}}$  peptide upfield shifts of 0.02, 0.01, and 0.01 ppm were seen after 44 h incubation. The latter peak movements took place over shorter incubation times, because the  $A\beta(1-42)$  peptide has enhanced  $\beta$ -aggregation rates. The most pronounced movements of the histidine 2H occurred during the first 40 h incubation with the  $A\beta(1-40)\text{Met35}^{\text{red}}$ , while comparable movements occurred with the  $A\beta(1-42)\text{Met35}^{\text{red}}$  peptide within the first 10 h. With the exception of the loss in signal/noise, no other spectral changes were observed, except for some minor peak movements within

(63) Wang, Y.; Jardetzky, O. *Protein Sci.* **2002**, *11*, 852–861.

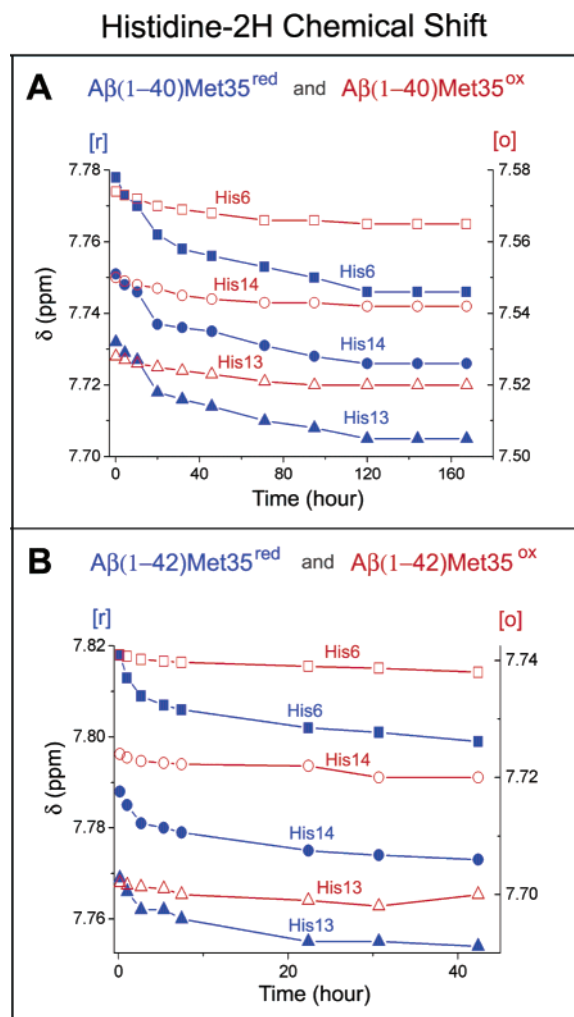


**Figure 7.** Graphical representations showing changes of the histidine 2H NMR chemical shifts that occur during incubation at 37 °C. (A)  $A\beta(1-40)Met35^{red}$  (blue) and  $A\beta(1-40)Met35^{ox}$  (red) and (B)  $A\beta(1-42)Met35^{red}$  (blue) and  $A\beta(1-42)Met35^{ox}$  (red) (0.20 mM, pH 7.2, buffered  $D_2O$  solution). To facilitate comparison, the graphs are presented with two y-axes: left y-axis for the  $Met35^{red}$  and right y-axis for the  $Met35^{ox}$  peptides.

the 2.60–3.00 ppm region. These latter chemical shift changes could be from the  $\beta CH_2$  side chains of the aspartic acid, asparagines, or the  $\epsilon CH_2$  of the lysine residues. Additional studies for identification of the residues responsible for these movements are currently underway.

## Discussion

The  $A\beta$  peptide is a normal physiologic constituent that from certain age-related microenvironmental changes undergoes  $\beta$ -aggregation and fibrillation. These self-assembly processes involve a conformational conversion from soluble, monomeric random structures into aggregated  $\beta$ -pleated sheet structures (random  $\rightarrow$   $\beta$ -strand), with the latter structure eventually precipitating as amyloid fibrils. Increasing research efforts are directed at detecting AD in its earliest stages, including those before it is clinically symptomatic. Knowledge of the structures and mechanisms associated with the early events of  $A\beta$  self-assembly would greatly facilitate the development of specific  $\beta$ -aggregation inhibitors that could ameliorate the effects associated with the  $A\beta$ -induced neurotoxicity.<sup>1,10–13</sup>

**Previous Solution NMR Studies of the  $A\beta$  Peptide.** The majority of earlier NMR reports utilized smaller-sized  $A\beta$

peptide fragments and/or aqueous solutions containing additives such as organic cosolvents or detergents, which as expected encourage mostly  $\alpha$ -helical structure.<sup>24,27–31,35</sup> These additives are presumably membrane mimicking and prevent  $\beta$ -aggregation, and hence are more conducive to NMR studies.

For conciseness, we restrict our discussion to previous NMR studies done in aqueous solution without additional cosolvents or detergents, which to the best of our knowledge include three reports of the following peptides:  $A\beta(12-28)$ ,<sup>33</sup>  $A\beta(10-35)$ ,<sup>32</sup>  $A\beta(1-40)Met35^{ox}$ ,<sup>34</sup> and  $A\beta(1-42)Met35^{ox}$ .<sup>34</sup> The NMR studies of the  $A\beta(12-28)$  fragment demonstrated that elevated temperatures promote a random  $\rightarrow$   $\beta$ -strand conversion localized at the Phe20–Ala21–Glu22 peptide region.<sup>33</sup> To some extent, these results agree with our work of the full length  $A\beta$  peptides, in that our CSI data show tendencies toward  $\beta$ -strand structure for regions containing both Phe20 and Ala21 (Figure 5).

Subsequent NMR studies showed that the  $A\beta(10-35)$  fragment adopts a collapsed coil (mostly random) with a well-defined central hydrophobic cluster (Leu17–Ala21) and turn- or bendlike structures (Asp7–Glu11 and Phe20–Ser26).<sup>32</sup> The  $A\beta(10-35)$  peptide was used instead of the full length 40- and 42-peptides, because it has greater solubility, adheres to preexisting amyloid plaques, and has  $^1H\alpha$  chemical shifts nearly identical to those of the  $A\beta(1-40)Met35^{red}$  (this implies that the  $A\beta(10-35)$  and  $A\beta(1-40)$  peptides have similar structures). Our NOE and NH temperature coefficient data (Figure 4) demonstrate that the full length  $A\beta$  peptides with  $Met35^{red}$  have similar tendencies for bend- or turnlike structures at Asp7–Glu11 and Phe20–Ser26; however, we did not observe a collapsed coil structure, nor did we see numerous long-range NOE interactions, such as between the aromatic ring of Tyr10 and the methyl group of Ala21.<sup>32</sup> These differences are probably due to the different peptide lengths and/or solution conditions (i.e., the NMR studies of the  $A\beta(10-35)$  were conducted at pH 5.7, while the present studies were done at pH 7.2).

The third report performed NMR studies of the  $A\beta(1-40)Met35^{ox}$  and  $A\beta(1-42)Met35^{ox}$  peptides in aqueous Tris–HCl buffered solutions at pH 6.4–8.2,<sup>34</sup> and the major conclusion was that both peptides adopt primarily nonglobular structures that deviate from random coil behavior with bendlike structures in the Ser8–Val12 and Phe20–Val24 regions. In addition,  $^{15}N\{^1H\}$  NOE data showed that the  $A\beta(1-42)Met35^{ox}$  has reduced flexibility at the C-terminus relative to the  $A\beta(1-40)Met35^{ox}$ . For the most part, these conclusions agree with our results, in that at pH 7.2 the  $A\beta$  peptides are largely random, but have proclivity toward bend- or turnlike structures in nearly identical regions. Additionally, the previously reported<sup>34</sup> decreased flexibility of the  $A\beta(1-42)Met35^{ox}$  C-terminus is consistent with our CSI data, in which the  $A\beta(1-42)Met35^{ox}$  C-terminus is more structured than that of the  $A\beta(1-40)Met35^{ox}$  (Figure 5). However, we saw fewer medium-range NOEs, and we did not observe rapid aggregation/precipitation of the  $A\beta(1-42)Met35^{ox}$  at 4 °C. These inconsistencies may be partly due to the different sample preparation procedures and/or solution conditions. For the previous studies,<sup>34</sup> the NMR measurements were done at pH 6.4–8.2, while all of our work was done at pH 7.2. Because the  $A\beta$  aggregation and precipitation is strongly enhanced below pH 7,<sup>16,64,65</sup> it is possible that  $A\beta$  seeds<sup>17,36</sup>

(64) Fraser, P. E.; Nguyen, J. T.; Surewicz, W. K.; Kirschner, D. A. *Biophys. J.* **1991**, *60*, 1190–1201.

were present in the previously reported NMR samples.<sup>34</sup> If present, these seeds can promote  $\beta$ -strand structure/aggregation and are sometimes unknowingly present. With our sample disaggregation protocol (see Experimental Procedures), all seeds were effectively removed, and the pH never dropped below 7.2, thus preventing seed-induced  $\beta$ -strand structure formation and aggregation.

**Comparison of the NMR Data for the  $A\beta$ Met35<sup>red</sup> and  $A\beta$ Met35<sup>ox</sup> Peptides.** We and others previously established that oxidation of the Met35 side chain inhibits  $\beta$ -aggregation and fibrillation of the  $A\beta(1-40)$  and  $A\beta(1-42)$  peptides<sup>24-26</sup> and that the inhibition may be due to the increased polarity imparted by the Met35 sulfoxide at the hydrophobic C-terminus (residues 29-40 and 29-42). The present NMR data now establish that this inhibition is more complicated and is not just confined to the C-terminus.

The NMR data demonstrate that the  $A\beta$  peptides adopt predominantly random extended chain structures, with residual local structures that could be early folded motifs in  $\beta$ -aggregation and amyloid formation. The  $A\beta$  peptides with Met35<sup>red</sup> have more regions that deviate from random coil structure, as shown by the CSI data and the greater amounts of short- and medium-range NOE connections. The extra NOEs are predominantly located in the Asp7-Glu11 and Asp23-Ser26 regions, which include one  $\alpha N(i,i+3)$  and three  $\alpha N(i,i+2)$  NOEs (Figure 4). In addition, all of the NH temperature coefficients for the  $A\beta(1-40)$ Met35<sup>ox</sup> are larger than 5 (indicative of weak NH backbone hydrogen bonding), while the  $A\beta(1-40)$ Met35<sup>red</sup> has two NH temperature coefficients less than 5 (Glu11 and Ser26). These data suggest that the  $A\beta(1-40)$ Met35<sup>red</sup> is more predisposed to forming turn- or bendlike structures centered at Asp7-Glu11 and Asp23-Ser26, similar to those seen with the  $A\beta(10-35)$  peptide.<sup>32</sup> Interestingly, turn- or bendlike structures are common structural motifs in unfolded states of proteins and peptide fragments.<sup>66</sup>

The CSI <sup>13</sup>C $\beta$  data establish that all peptides, except the  $A\beta(1-40)$ Met35<sup>ox</sup>, show tendency toward  $\beta$ -strand structure in the central hydrophobic region, which includes Leu17-Ala21, Leu17-Phe20, and Val18-Phe20 for the  $A\beta(1-42)$ Met35<sup>red</sup>,  $A\beta(1-40)$ Met35<sup>red</sup>, and  $A\beta(1-42)$ Met35<sup>ox</sup> peptides, respectively. Noticeably, the lengths of these regions are consistent with the relative peptide  $\beta$ -aggregation rates:  $A\beta(1-42)$ Met35<sup>red</sup> (5 residues, most aggregation prone) >  $A\beta(1-40)$ Met35<sup>red</sup> (4 residues) >  $A\beta(1-42)$ Met35<sup>ox</sup> (3 residues) >  $A\beta(1-40)$ Met35<sup>ox</sup> (0 residues, least aggregation prone). The importance of the central hydrophobic region for  $\beta$ -aggregation has previously been noted,<sup>67-69</sup> and the core of the amyloid  $\beta$ -strand structure is composed of Leu17-Ala21.<sup>70</sup>

Regarding the hydrophobic C-terminus (residues 29-40 or 29-42), the CSI <sup>1</sup>H $\alpha$  data reveal that both 40-residue peptides have no inclination toward  $\beta$ -strand structure, whereas the

$A\beta(1-42)$ Met35<sup>red</sup> has two regions (Ile31-Val36 and Val39-Ile41) and the  $A\beta(1-42)$ Met35<sup>ox</sup> has one region (Val39-Ile41). The CSI <sup>13</sup>C $\beta$  data also show that the Val39-Val40-Ile41 favor  $\beta$ -sheet structure in the  $A\beta(1-42)$  and not the  $A\beta(1-40)$  peptide, regardless of the Met35 oxidation state (Figure 5). There are also differences in the NH chemical shifts (Figure 3), where oxidation causes six NH signals to shift with the  $A\beta(1-42)$  (Leu34-Met35-Val36-Gly37-Gly38-Val39), while only three residues with the  $A\beta(1-40)$  (Leu34-Met35-Val36). These results suggest that the hydrophobic C-terminus plays an important role in the amyloid associated random  $\rightarrow$   $\beta$ -sheet transition for the longer  $A\beta(1-42)$  and not the shorter  $A\beta(1-40)$  peptide, consistent with previous proposals.<sup>16,17</sup>

With the exception of the  $A\beta(1-40)$ Met35<sup>ox</sup>, the NMR data establish that the central hydrophobic region is important for  $\beta$ -aggregation for all peptides, plus the C-terminus is important with the longer 42-residue peptide,<sup>16,17,65</sup> and that Met35 oxidation perturbs both of these effects.

**Effect of the Met35 Oxidation State on the Histidine Chemical Shifts During Aging.** The unique structure of the imidazole ring enables histidine to be involved in metal binding, hydrogen bonding, and salt-bridging. Numerous reports have shown that the histidine residues have important roles in the  $A\beta$  aggregation into  $\beta$ -strand structures, possibly through histidine<sup>+</sup>-carboxylate<sup>-</sup> (Asp<sup>-</sup> or Glu<sup>-</sup>) salt-bridge formation<sup>3,71-73</sup> or by the  $A\beta$  binding to glycosaminoglycans,<sup>74</sup> copper,<sup>23,75</sup> zinc,<sup>75</sup> or Congo red.<sup>76</sup> For the present study, the possibility that the histidine NMR chemical shift movements may be caused by pH changes or metal binding is insignificant, because the pH of the NMR samples remained constant and all of the samples contained excess amounts of Na<sub>2</sub>EDTA that effectively removes trace metal contaminants.

The aging studies establish two important facts, that the histidine side chains play important roles in the  $A\beta$  self-assembly and that the Met35 oxidation state strongly influences the level of this contribution (Figure 7). With the  $A\beta(1-40)$ Met35<sup>red</sup> and the  $A\beta(1-42)$ Met35<sup>red</sup> peptides, the nearly identical chemical shift changes for the three histidines (His6, His13, and His14) suggest that they contribute equally and may be involved in similar reactions (Figure 8). The upfield shifts of the 2H correspond to a loss in the amount of protonated histidine, which, based on the experimentally determined pK<sub>a</sub> 6.5-6.6 value,<sup>77</sup> constitutes about 10-20% at pH 7.2. Because the histidine 2H NMR signals move upfield during the aggregation events, it seems reasonable to conclude that the movement corresponds to a loss in the amount of His-H<sup>+</sup> present in solution at pH 7.2 that is equilibrating with uncharged His. The loss in the amount of NMR-detectable His-H<sup>+</sup> could be from

- (65) Burdick, D.; Soreghan, B.; Kwon, M.; Kosmoski, J.; Knauer, M.; Henschen, A.; Yates, J.; Cotman, C.; Glabe, C. *J. Biol. Chem.* **1992**, *267*, 546-554.  
 (66) Dyson, H. J.; Wright, P. E. *Nat. Struct. Biol.* **1998**, 499-503.  
 (67) Hilbich, C.; Kisters-Woike, B.; Reed, J.; Masters, C. L.; Beyreuther, K. *J. Mol. Biol.* **1992**, *228*, 4609-4473.  
 (68) Esler, W. P.; Stimson, E. R.; Ghilardi, J. R.; Lu, Y.-A.; Felix, A. M.; Vinters, H. V.; Mantyh, P. W.; Lee, J. P.; Maggio, J. E. *Biochemistry* **1996**, *35*, 13914-13921.  
 (69) Pallitto, M. M.; Ghanta, J.; Heinzelman, P.; Kiessling, L. L.; Murphy, R. M. *Biochemistry* **1999**, *38*, 3570-3578.  
 (70) Inouye, H.; Kirschner, D. A. *The Nature and Origin of Amyloid Fibrils*; John Wiley & Sons: New York, 1996; Ciba Foundation Symposium, 22-39.

- (71) Fraser, P. E.; McLachlan, D. R.; Surewicz, W. K.; Mizzen, C. A.; Snow, A. D.; Nguyen, J. T.; Kirschner, D. A. *J. Mol. Biol.* **1994**, *244*, 64-73.  
 (72) Huang, T. H. J.; Fraser, P. E.; Chakrabarty, A. *J. Mol. Biol.* **1997**, *269*, 214-224.  
 (73) Tjernberg, L. O.; Callaway, D. J.; Tjernberg, A.; Hahne, S.; Lilliehook, C.; Terenius, L.; Thyberg, J.; Nordstedt, C. *J. Biol. Chem.* **1999**, *274*, 12619-12625.  
 (74) Giulian, D.; Haverkamp, L. J.; Yu, J.; Karshin, W.; Tom, D.; Li, J.; Kazanskaia, A.; Kirkpatrick, J.; Roher, A. E. *J. Biol. Chem.* **1998**, *273*, 29719-29726.  
 (75) Curtain, C. C.; Ali, F.; Volitakis, I.; Cherny, R. A.; Norton, R. S.; Beyreuther, K.; Barrow, C. J.; Masters, C. L.; Bush, A. I.; Barnham, K. J. *J. Biol. Chem.* **2001**, *276*, 20466-20473.  
 (76) Inouye, H.; Nguyen, J.; Fraser, P.; Shinchuk, L.; Packard, A.; Kirschner, D. *Amyloid: Int. J. Exp. Clin. Invest.* **2000**, *7*, 179-188.  
 (77) Ma, K.; Clancy, E. L.; Zhang, Y.; Ray, D. G.; Wollenberg, K.; Zagorski, M. G. *J. Am. Chem. Soc.* **1999**, *121*, 8698-8706.

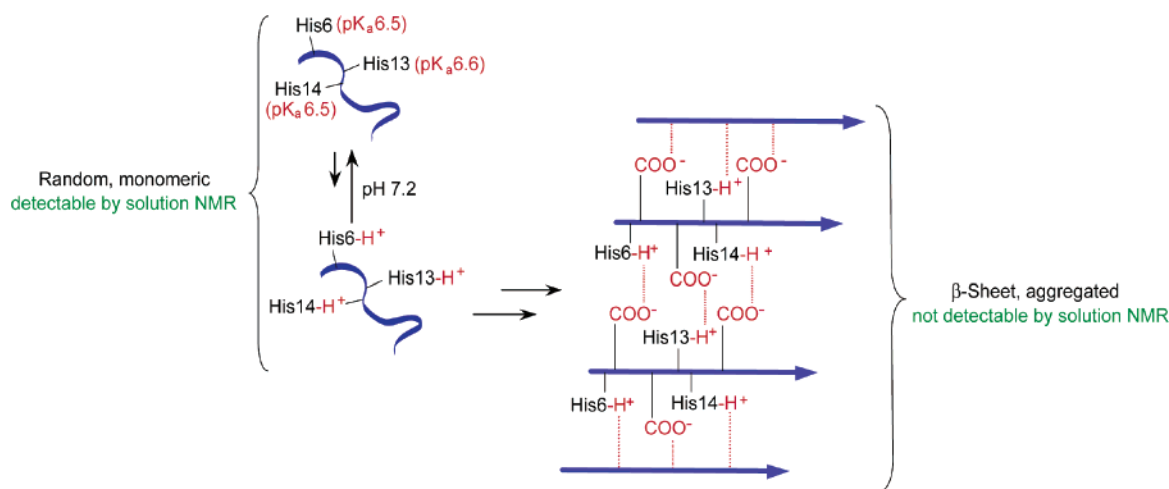


**Figure 8.** Proposed mechanism to account for the age-induced upfield shifts of the histidine 2H NMR signals (NMR data shown in Figure 7). The His6, His13, and His14 side chains have comparable  $pK_a$  values,<sup>77</sup> and at pH 7.2 they exist in equilibrium between protonated and unprotonated states (the latter predominates), and both appear as the same time-averaged NMR signal. As aggregation ensues, the side chains of the aspartic acid or glutamic acid residues bond with the protonated histidines to form intermolecular salt-bridges that are important for stabilizing the non-NMR detectable  $\beta$ -strand aggregates.<sup>3,71–73</sup> The loss of protonated histidine causes the average NMR signal to shift upfield.

its involvement in aggregation. The larger and more gradual upfield chemical shift movements seen with the A $\beta$ (1–40)-Met35<sup>red</sup> suggest that histidine side chains serve an important and protracted role in  $\beta$ -aggregation. This conclusion is supported by comparison of the static (without aging) histidine–2H chemical shifts (Figure 6). For the His6, His14, and His13, oxidation of the Met35 side chain promotes upfield shifts of 0.22, 0.28, and 0.30 ppm in the A $\beta$ (1–40) (Figure 6A), but only 0.06–0.07 ppm differences for the A $\beta$ (1–42) peptide (Figure 6B).

During aging, the observation of additional peak movements in the 2.60–3.00 ppm region (data not shown) suggests that the side chains of the aspartic acid residues could be involved in reactions with the histidines, such as by His<sup>+</sup>–Asp<sup>–</sup> salt-bridging (the chemical shift of the Asp- $\beta$ CH<sub>2</sub> is 2.6–2.9 ppm). To determine whether the aspartic acid residues are indeed forming salt-bridges with the histidines, additional studies with selectively <sup>13</sup>C- and <sup>15</sup>N-labeled aspartic acid residues are currently underway.

**Influence of the Met35 Oxidation State on the Mechanism of  $\beta$ -Amyloidosis.** We previously established that oxidation of the Met35 side chain disrupts the normal A $\beta$  fibrillation events by preventing formation of the amyloid protofibril and other mature fibrils.<sup>26</sup> The present NMR results, along with other recent chemical studies using a novel photoinduced cross-linking procedure,<sup>78</sup> suggest that this disruption may occur during the early stages of A $\beta$  assembly and that the A $\beta$ (1–40)Met35<sup>red</sup>, A $\beta$ (1–40)Met35<sup>ox</sup>, A $\beta$ (1–42)Met35<sup>red</sup>, and A $\beta$ (1–42)Met35<sup>ox</sup> peptides may aggregate by different pathways.

In general, the driving force for  $\beta$ -aggregation and fibrillation is hydrophobic, with electrostatic interactions playing an important but secondary role.<sup>8,71,79</sup> In the early stages of  $\beta$ -aggregation, monomers adopt partially structured conformations, which in turn associate to form spherical aggregates that act as seeds and accrete more monomers to form larger

neurotoxic aggregates. In the subsequent fibrillation stages, the larger aggregates assemble together (laterally or end-to-end), producing protofibrils that with further maturation form Type I and Type II amyloid fibrils.<sup>79</sup> Although progress has been made in the characterization of the fibril structures, very little is known about the early formed, partially structured conformations, including the residues and side chains involved in the self-association processes.

Shown in Figure 9 is a hypothetical scheme for the A $\beta$  self-assembly process, in which the NMR-detectable events correspond to unfolded or partly folded monomers, which lead to the production of small soluble aggregates and eventually the larger less soluble amyloid fibrils. In solution, the A $\beta$  peptide exists as an ensemble of rapidly equilibrating conformations (monomeric random extended, aggregated  $\beta$ -strand, turns, bends, or kinks), in which the NMR-detectable data correspond to monomeric peptide, that based on the CSI and NOE data fit with a predominantly random extended chainlike structure. However, within the ensemble, if a particular peptide region is leaning more toward aggregated  $\beta$ -strand (instead of just random structure), then the average CSI and NOE data should reflect these changes.

On the basis of the present NMR results and other experimental data, we propose that different early association processes occur with the four A $\beta$  peptides investigated herein. In the first step, the four A $\beta$  peptides undergo different residue-specific, hydrophobic association with accompanying turn- or bendlike formation, while in the second step electrostatic association occurs, in which the histidine side chains play important roles in stabilizing the fibrils (possibly by salt-bridging). The residues involved in the hydrophobic association were selected from their predisposition for  $\beta$ -strand structure (Figure 5), and the turn- or bendlike structures (Asp7–Glu11 and Phe20–Ala30) follow from medium-range NOE connectivities (Figure 4). This scheme implies that, in the first steps of A $\beta$  assembly, both hydrophobic and bendlike structures are required to produce amyloid fibrils. Thus, the A $\beta$ (1–40)Met35<sup>ox</sup> peptide, which shows the least tendency for turn- or bendlike structures and essentially no  $\beta$ -strand structure, is the least likely to aggregate and does

(78) Bitan, G.; Kirkitadze, M. D.; Lomakin, A.; Vollers, S. S.; Benedek, G. B.; Teplow, D. B. *Proc. Natl. Acad. Sci. U.S.A.* **2003**, *100*, 330–335.

(79) Rochet, J. C.; Lansbury, P. T., Jr. *Curr. Opin. Struct. Biol.* **2000**, *10*, 60–68.

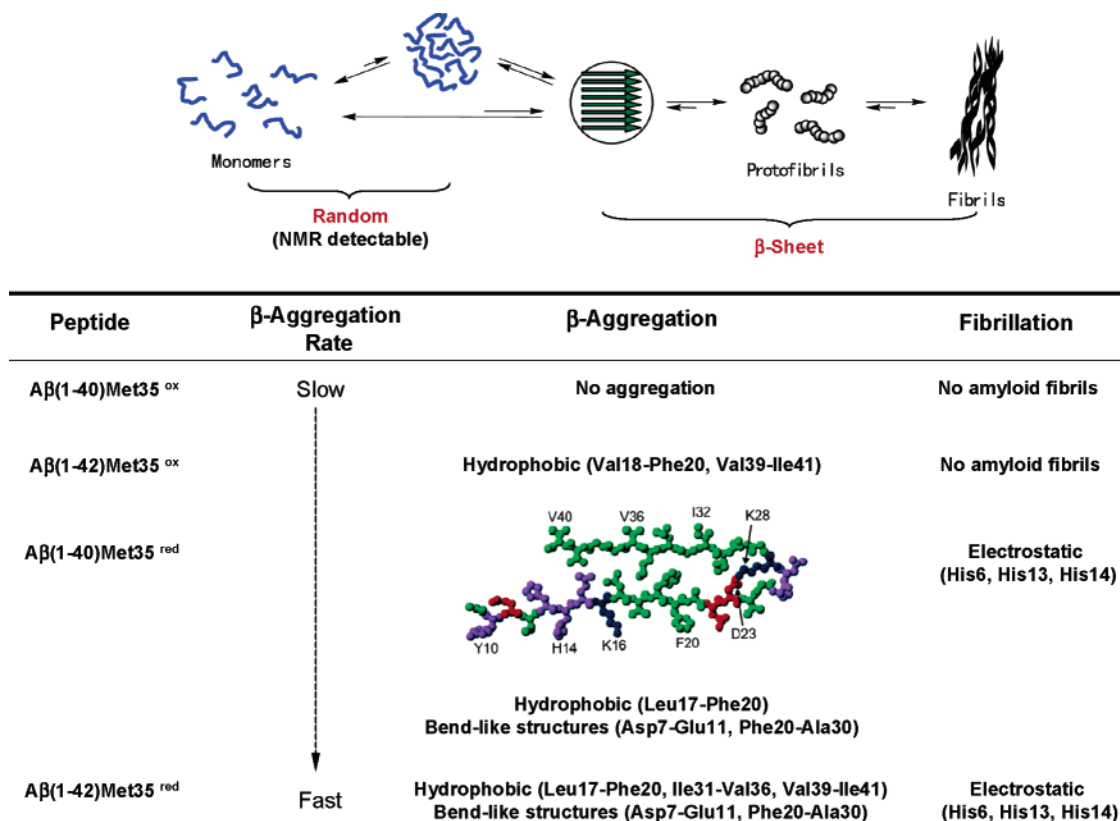


**Figure 9.** Schematic model showing the equilibrium among the different A $\beta$  aggregation states, which include disordered aggregates, soluble  $\beta$ -strand aggregates shown with parallel orientations,<sup>4,5</sup> later-stage protofibrils, and end-stage fibrils. Solution NMR signals detect only the early stages of association, that is, monomeric peptide where the chemical shifts, NOE distances, and signal/noise are influenced by the relative distribution among the various states. Freshly prepared peptide solutions kept at 0–5 °C remain as largely unassociated monomers, whereas aging at 37 °C will shift the distribution toward the  $\beta$ -aggregated states. The residue-specific interactions taking place during the first step of A $\beta$  self-assembly and second stage  $\beta$ -strand fibrillation are shown in the table (selected on the basis of the present NMR and other experimental data) and indicate that certain localized peptide regions are predisposed toward  $\beta$ -strand and bendlike structures. The four A $\beta$  peptides investigated in this study have different  $\beta$ -aggregation rates and interactions, with the oxidation state of the methionine-35 playing an influential role. In the first step, all of the pathways involve hydrophobic association, followed by electrostatic association of the histidine side chains. The pathway of the A $\beta$ (1–40)Met35<sup>red</sup> peptide incorporates a single, central molecule taken from a larger working model of the cross- $\beta$  unit that has in-register parallel  $\beta$ -sheets formed by residues 12–24 and 30–40 (based on solid-state NMR data) and a bend or kink for residues 25–29 (put forth by Tycko and co-workers).<sup>5</sup> In this single molecule representation, a possible stabilizing hydrophobic interaction exists between the  $\epsilon$ CH<sub>3</sub>–Met35 and the Phe19 aromatic ring (5–6 Å), which could become disrupted by methionine oxidation and thus account for the inability of the A $\beta$ (1–40)Met35<sup>ox</sup> to undergo  $\beta$ -aggregation and fibrillation.

not form amyloid fibrils. On the other extreme, the A $\beta$ (1–42)Met35<sup>red</sup> peptide has turn- or bendlike tendencies and has the greatest number of residues favoring  $\beta$ -strand structure, and consequently undergoes very rapid  $\beta$ -aggregation. Because the Met35<sup>red</sup>  $\rightarrow$  Met35<sup>ox</sup> conversion blocks critical hydrophobic association in the first step, intermolecular electrostatic association cannot take place in the second step, thus accounting for the lack of histidine 2H NMR signal movement with the A $\beta$  peptides containing Met35<sup>ox</sup>. Further support of this scheme comes from work with other proteins, in that well-defined initial secondary structures are not required for amyloidosis, but rather the type of intermolecular interactions (hydrophobic and electrostatic) involved in the association processes.<sup>8,9</sup>

We also propose that the pathway involved with assembly of the A $\beta$ (1–40)Met35<sup>red</sup> peptide includes a molecular model containing an intramolecular  $\beta$ -strand structure that was made on the basis of solid-state NMR (Figure 9).<sup>5</sup> The model is based on solid-state NMR constraints and has Val12–Val24 and Ala30–Val40 adopting a parallel  $\beta$ -strand connected by a bend within the Gly25–Gly29 region. Our solution NMR data show medium-range NOEs throughout the Phe20–Ala30 region that

probably exist as an ensemble of rapidly interconverting random structures with kink- or bendlike propensities, which in the fibril forms a single kink at Gly25–Gly29 in accordance with solid-state NMR.<sup>5</sup> Thus, if the solid-state NMR model is part of a rapidly equilibrating ensemble in solution, it can provide a rationale for the Met35<sup>ox</sup> inhibition to  $\beta$ -aggregation. In the model, the Met35  $\epsilon$ CH<sub>3</sub>S group is proximate to the center of the Phe19 aromatic ring (5–6 Å), which represents a hydrophobic interaction that may be critical to the stability of the  $\beta$ -strand structure. The importance of this interaction is supported from other studies, where A $\beta$  peptide analogues without Phe19, Phe20, or Met35 do not produce  $\beta$ -amyloid deposits.<sup>67,68,80</sup> The increased polarity of the Met35 sulfoxide ( $\epsilon$ CH<sub>3</sub>S=O) may destabilize this interaction and thus provide a rationale for the lack of  $\beta$ -aggregation of the A $\beta$ (1–40)Met35<sup>ox</sup> peptide. Interestingly, previous NMR studies of the A $\beta$ (1–40)Met35<sup>red</sup> and A $\beta$ (1–40)Met35<sup>ox</sup> in water–micelle solution<sup>24</sup> showed that the nonpolar Met35<sup>red</sup> side chain is confined to the hydrophobic  $\alpha$ -helix, while the more polar Met35<sup>ox</sup> side chain is repositioned for better contact with the aqueous solution. To

(80) Lorenzo, A.; Matsudaira, P.; Yankner, B. A. *Soc. Neurosci. Abstr.* **1993**, *19*, 184.

substantiate the proposed pathways, additional NMR studies using A $\beta$  peptides with site-specific  $^{13}\text{C}$  and  $^{15}\text{N}$  labels are currently underway in our laboratory.

**Acknowledgment.** This work was supported in part by grants from the NIH (AG-14363-04) and the American Health Assistance Foundation (A2000-056). We thank Frank Sönnichsen, Jeff Kelly, Bob Griffin, Rob Friedland, Larry Sayre, and Witold Surewicz for helpful discussions, as well as Erik Zuiderweg,

Jim Prestegard, and John Glushka for use of the NMR Facility at the University of Michigan and the University of Georgia. We also thank T. D. Goddard and D. G. Kneller for use of the SPARKY 3 software program, Rob Tycko for use of his A $\beta$ (1–40) peptide model, and Jeff Kelly and Hillal Lashuel for communication of unpublished results from sedimentation velocity measurements of the A $\beta$  peptide.

JA036813F